Modeling large scale shoreline sand waves under oblique wave incidence

N. van den Berg,[1] A. Falqués,[1] and F. Ribas[1]

Received 1 August 2011; revised 22 June 2012; accepted 29 June 2012; published 17 August 2012.

[1] The hypothesis that the formation and dynamics of large scale shoreline sand waves can be explained by a feedback mechanism between waves and nearshore morphology under very oblique wave incidence is explored with a quasi 2D nonlinear morphodynamic model. Using constant wave conditions it is found that if the wave incidence angle at the depth of closure is larger than about 45° the rectilinear coastline becomes unstable and a shoreline sand wavefield develops from small random perturbations. Shoreline sand waves develop with wavelengths between 2 and 5 km, they migrate downdrift at about 0.5 km/yr and they reach amplitudes up to 120 m within 13 years. Larger wave obliquity, higher waves and shorter wave periods strengthen the shoreline instability. Cross-shore transport is essential for the instability and faster cross-shore dynamics leads to a faster growth of the sand waves. Simulations with variable wave incidence angles (alternating between 60° and 30°) show that a large proportion of high angle waves is required for spontaneous sand wave formation (at least 80%). Insight is provided into the physical mechanism behind high angle wave instability and the occurrence of a optimal length scale for sand wave growth. The generic model results are consistent with existing observations of shoreline sand waves, in particular with those along the southwest coast of Africa.

Citation: van den Berg N., A. Falqués, and F. Ribas (2012), Modeling large scale shoreline sand waves under oblique wave incidence, *J. Geophys. Res.*, *117*, F03019, doi:10.1029/2011JF002177.

1. Introduction

[2] Shoreline undulations are episodically or persistently found along many sandy coasts. A well known example are megacusps, associated with surfzone rhythmic sandbars and rip channels, with a typical alongshore length scale of $O(10^2$ m) and a timescale of $O(10^1$ day) [*Short*, 1999]. The formation and dynamics of these rhythmic patterns have been explained as a self-organized behavior of the morphodynamic system [*Coco and Murray*, 2007]. The patterns are not simply dictated by a template in the hydrodynamic forcing but they emerge from the feedback between morphology and hydrodynamics via sediment transport and they posses their own characteristic length and timescales [e.g., *Garnier et al.*, 2008; *Castelle et al.*, 2010].

[3] In the present study we will focus on shoreline undulations with a larger alongshore length scale $O(10^3$ m) and a longer timescale $O(10^3$ day). These large scale undulations have been observed on various coasts around the world [see, e.g., *Bruun*, 1954; *Stewart and Davidson-Arnott*, 1988; *Verhagen*, 1989; *Thevenot and Kraus*, 1995; *Gravens*, 1999; *Guillen et al.*, 1999; *Ruessink and Jeuken*, 2002; *Davidson-Arnott and van Heyningen*, 2003; *Alves*, 2009; *Ryabchuk et al.*, 2011; *Kaergaard et al.*, 2012]. They are in general unrelated to surfzone sandbars and they will be referred to as large scale shoreline sand waves or simply sand waves. Sand waves cause a spatial and temporal variability of the shoreline position that can be greater than the uniform trend and their dynamics are therefore of great importance for coastal management [*Stive et al.*, 2002].

[4] A potential mechanism for the formation and dynamics of sand waves was provided by *Ashton et al.* [2001]. They showed that a rectilinear sandy coast exposed to very oblique wave incidence (angle of wavefronts in deep water with respect to coastline orientation larger than a critical angle, $\theta \simeq 42°$) may be unstable leading to the formation of sand waves, cuspate features and spits (hereinafter referred to as high angle wave instability or HAWI). Although there are no direct observations of this instability working in nature (an important difficulty is the large length and time scales), coastlines with a wave climate dominated by very oblique incidence commonly feature large scale undulations, suggesting that this instability could be responsible for the formation of sand waves [*Ashton and Murray*, 2006b; *Falqués*, 2006; *Medellín et al.*, 2008; *Ryabchuk et al.*, 2011; *Kaergaard et al.*, 2012].

[5] The approach of *Ashton et al.* [2001] is based on the reasonable assumption that, for the description of shoreline changes on a large temporal and spatial scale (at least one order of magnitude bigger than that of rip channels and the rhythmicity of surfzone bars), the one-line shoreline modeling concept can be applied and that the details of surfzone

[1]Applied Physics Department, Technical University of Catalonia, Barcelona, Spain.

Corresponding author: N. van den Berg, Applied Physics Department, Technical University of Catalonia, Campus Nord UPC B5, E-08034 Barcelona, Spain. (niels@fa.upc.edu)

0148-0227/12/2011JF002177

morphodynamics can be ignored. The changes in shoreline position are simply governed by the gradients in the total alongshore transport rate Q (m^3/s) driven by obliquely breaking waves [*Komar*, 1998]. Negative gradients in Q lead to shoreline advance (deposition) and positive gradients lead to shoreline retreat (erosion). It is assumed that on a long timescale the cross-shore profile attains an equilibrium shape and that it shifts together with the shoreline position. Therefore, when an undulation is present in the shoreline, the bathymetric lines follow this undulation. Q is commonly described as a function of the wave height, H_b, and the angle between the wavefronts at breaking and the shoreline orientation, $\alpha_b = \theta_b - \phi$ (e.g., CERC formula) [*Komar*, 1998]. However, H_b and θ_b can not be considered external parameters for shoreline evolution. When an undulation is present in the shoreline, refraction over the associated bathymetry leads to alongshore gradients in θ_b and refractive wave energy spreading leads to alongshore gradients in H_b. This feedback between the shoreline changes, the associated bathymetry and the wavefield is the essential physical mechanism behind HAWI. For low wave incidence angles ($\theta \lesssim 42°$) the gradients in α_b are dominant for Q and they cause a positive transport gradient along a shoreline perturbation, which leads to diffusion of the perturbation and a stable shoreline. However, for high wave incidence angles ($\theta \gtrsim 42°$) the gradients in H_b become dominant for Q and they cause a negative transport gradient along a shoreline perturbation, which leads the growth and migration of the perturbation and therefore an unstable shoreline [*Ashton and Murray*, 2006a, 2006b; *Falqués and Calvete*, 2005; *Falqués et al.*, 2011a].

[6] *Ashton et al.* [2001] used a cellular shoreline model and in order to include the feedback mechanism associated to HAWI they defined Q in terms of the wave height and angle at the base of the shoreface, before nearshore wave transformation takes place. This depth is equivalent to the wave base and here the wave height and angle are independent of the shoreline and we refer to them as deep water waves (H_∞ and θ_∞). A crucial step in this approach is the computation of H_b and θ_b as a function of H_∞, θ_∞, the wave period (T) and the nearshore bathymetry. To this end, they assumed: i) wave transformation over rectilinear depth contours that are parallel to the evolving shoreline and ii) that any gradient in the alongshore transport leads to an instantaneous shift of the whole cross-shore profile. Assumption i is inconsistent with the undulating shape of the bathymetry and, most importantly, it assumes indirectly that shoreline undulations extend offshore in the bathymetry down to the wave base. Assumption ii restricts the applicability of the model to large timescales (much larger than the reaction time of the cross-shore beach profile) and both assumptions are only suitable in the limit of very large scale features. A validation of the main results of this study requires a model that can describe bathymetric perturbations with a finite offshore extent and curvilinear depth contours.

[7] A linear stability analysis with these two characteristics was presented by *Falqués and Calvete* [2005]. They found that instability could still develop, provided that the offshore extent of the perturbations in the bathymetry, which was a free parameter in their analysis, was large enough. Furthermore, the range of unstable angles was significantly reduced for long period waves. Thus, the critical angle proposed by *Ashton et al.* [2001], $\theta_\infty \simeq 42°$, is actually a lower bound and instability in general requires larger angles and short wave periods. A very important output of the linear stability analysis was a wavelength selection for the initial development of the shoreline sand waves, $\lambda \sim 3$–15 km [see also *Uguccioni et al.*, 2006]. This is one order of magnitude larger than that of surfzone instabilities and, together with the characteristic growth time predicted by the model, O (1 yr), it confirms that the one-line approach is appropriate for dealing with HAWI. Although the study of *Falqués and Calvete* [2005] confirmed the existence of HAWI and provided some new insight, it had several limitations. First, it relied on the assumption of an instantaneous reaction of the bathymetry to shoreline changes (assumption ii above). Furthermore, the offshore extent of the bathymetric perturbations was fixed beforehand. This is a crude approximation as in nature this distance is dynamic. Finally, a basic assumption of the linear stability analysis is that the amplitude of the sand waves was considered to be small and the analysis does not describe the actual evolution of the sand waves and possible nonlinear effects.

[8] *Van den Berg et al.* [2011] used a nonlinear quasi 2D morphodynamic model to study the evolution of nourished beaches under high angle wave incidence. This model is an extension of the linear model of *Falqués and Calvete* [2005]. It can describe shoreline undulations with a large amplitude and a parametrization of cross-shore dynamics was introduced. Because of the latter, the coupling between the shoreline and the bathymetry is no longer instantaneous and the offshore extent of the bathymetric perturbations is dynamic. In the present study this model is used to investigate the formation and dynamics of shoreline sand waves. In particular, we investigate to what extent the predictions of *Ashton et al.* [2001] and *Falqués and Calvete* [2005] depend on their idealizations and we look at new aspects of sand wave dynamics that were not caught by the previous models. The influence of wave height and period, the important role of cross-shore transport and the effect of variable wave incidence angles are investigated. Furthermore, new insight is provided into the physical mechanism behind HAWI and the wavelength selection and we compare the generic results with observations, from a qualitative point of view.

2. Model

[9] The Q2D-morfo model is a nonlinear morphodynamic model for large scale shoreline dynamics. A cartesian frame with horizontal coordinates x, y and upward vertical coordinate z is used, where y runs along the initial mean shoreline orientation. The nearshore region is represented by a rectangular domain, $0 < x < L_x$, $0 < y < L_y$. The unknowns are the moving shoreline, $x = x_s(y, t)$, and the changing bed level, $z = z_b(x, y, t)$. The dynamic equation for the bed level is the sediment mass conservation:

$$\frac{\partial z_b}{\partial t} + \frac{\partial q_x}{\partial x} + \frac{\partial q_y}{\partial y} = 0, \tag{1}$$

where $\vec{q} = (q_x, q_y)$ is the depth integrated sediment flux and the bed porosity factor is included for convenience in $\vec{q}$. The shoreline position is determined by interpolating between the cells with $z_b > 0$ and the cells with $z_b < 0$.

2.1. Sediment Transport

[10] Nearshore 2D depth average models compute the sediment flux from the wavefield and the mean hydrodynamics (currents). In contrast, the present model computes the sediment transport directly from the wavefield via parameterizations without determining the mean hydrodynamics. It is this important simplification that makes this model capable of performing large scale simulations with a reasonably low computational cost. The dynamics of small scale surfzone features like rhythmic bars and rip currents can however not be reproduced but this simplification seems reasonable in the context of large scale shoreline modeling.

[11] The sediment flux in the model is decomposed as

$$\vec{q} = \vec{q}_L + \vec{q}_C + \vec{q}_D. \tag{2}$$

The first term represents the littoral drift, which is due to the alongshore current driven by the breaking waves in case of off-normal wave incidence. It is evaluated by first computing the total sediment transport rate, i.e., the cross-shore integrated flux, with an extended version of the CERC formula [*Komar*, 1998]. The formula has been adapted to include a second term introduced by *Ozasa and Brampton*, 1980, which represents the contribution of alongshore gradients in wave height to the alongshore transport,

$$Q = \mu H_b^{5/2}\left(\sin(2\alpha_b) - \frac{2r}{\beta}\cos(\alpha_b)\,\frac{\partial H_b}{\partial y}\right), \tag{3}$$

where $H_b(y)$ is the root mean square wave height at breaking, $\alpha_b = \theta_b(y) - \phi(y)$ is the angle between wavefronts at breaking and the coastline and β is the mean surfzone slope. The constant μ is proportional to the empirical parameter K_1 of the original CERC formula. This parameter controls the magnitude of the transport and the default value μ = 0.2 $m^{1/2}$ s^{-1} roughly corresponds to $K_1 = 0.7$. The constant $r = K_2/K_1$, where K_2 is the empirical parameter of the second term. The default value of $r = 1$ is used, which is equivalent to $K_2 = K_1$. Then, the sediment flux is computed by multiplying the total transport rate by a normalized shape function $f(x)$, qualitatively based on the cross-shore profile of the alongshore current [*Komar*, 1998]:

$$\vec{q}_L = f(x - x_s(y))Q(y)(\sin\phi(y), \cos\phi(y)), \tag{4}$$

with

$$f(x) = \frac{4}{\sqrt{\pi}L^3}x^2 e^{-(x/L)^2}, \tag{5}$$

where $L = 0.7X_b(y)$ and $X_b(y) = x_b(y) - x_s(y)$ is the width of the surfzone. The point of breaking, $x_b(y)$, is the most offshore point where $H(x, y) \geq \gamma_b D(x, y)$. D is the water depth and γ_b is the breaking index (the ratio wave height to water depth at breaking).

[12] The orientation of the coast, ϕ, is represented by the mean orientation of the bathymetric contours in the surfzone with respect to the y-axis rather than the orientation of the coastline itself. This seems more appropriate because it is this orientation that actually affects the waves at breaking. It is computed as

$$\sin\phi(y) = \overline{\frac{\partial z_b}{\partial y}} \Big/ \sqrt{\left(\overline{\frac{\partial z_b}{\partial x}}\right)^2 + \left(\overline{\frac{\partial z_b}{\partial y}}\right)^2}, \tag{6}$$

where the average is computed within a rectangular box with a cross-shore length L_{box}, an alongshore length 2 * L_{box}, where $L_{box} = B * X_b$ and the default value of the constant B is 2.

[13] *Ashton and Murray* [2006a] explored other formulas for breaking-wave-driven transport and found that all formulas show the potential for shoreline instability but that they may predict somewhat different shoreline responses under the same conditions. An interesting study by *List and Ashton* [2007] demonstrated that the cross-shore integrated alongshore transport computed with a process-based wave, circulation, and sediment transport model showed patterns along an undulating shoreline similar to the transport computed directly from the wavefield with the CERC formula. Even though they did not compute morphological evolution, the process based model predicted the potential for high angle wave instability, confirming that the present simplified approach using the CERC formula can be used for the exploration of HAWI. However, care must be taken when mathematical models like the CERC formula are used for quantitative predictions of alongshore transport and the resulting shoreline change [*Cooper and Pilkey*, 2004]. In this study we only look at the qualitative behavior and the use of CERC formula therefore seems valid.

[14] The second term in equation (2) is a parametrization of cross-shore sediment transport processes. We assume that, on a relatively long timescale, these processes drive the cross-shore profile to an equilibrium profile z_{be}, so that

$$\vec{q}_C = -\gamma_x\left(\frac{\partial(z_b - z_{be})}{\partial x}, 0\right), \tag{7}$$

where $z_{be}(x, y) = Z(x - x_s(y))$ is the assumed equilibrium profile and γ_x is a cross-shore diffusivity coefficient. The third term in equation (2) is an alongshore diffusive transport that suppresses the growth of small scale noise,

$$\vec{q}_D = -\gamma_y\left(\frac{\partial z_b}{\partial x}\sin\phi + \frac{\partial z_b}{\partial y}\cos\phi\right)(\sin\phi, \cos\phi). \tag{8}$$

The physical basis for the coefficients γ_x and γ_y is the diffusivity caused by wave breaking. Thereby, they depend on the wave energy dissipation and their order of magnitude has been estimated by using the expression for momentum mixing due to wave breaking [*Battjes*, 1975],

$$\nu_t = M(\mathcal{D}/\rho)^{1/3}H, \tag{9}$$

where M is a non-dimensional constant ($O(1)$), $\mathcal{D}$ is the wave energy dissipation per time and area unit, ρ is the water density and H is the root mean square wave height. We assume that γ_x and γ_y scale with ν_t, with $H = H_b$ in equation (9). The order of magnitude of $\mathcal{D}$ can be estimated

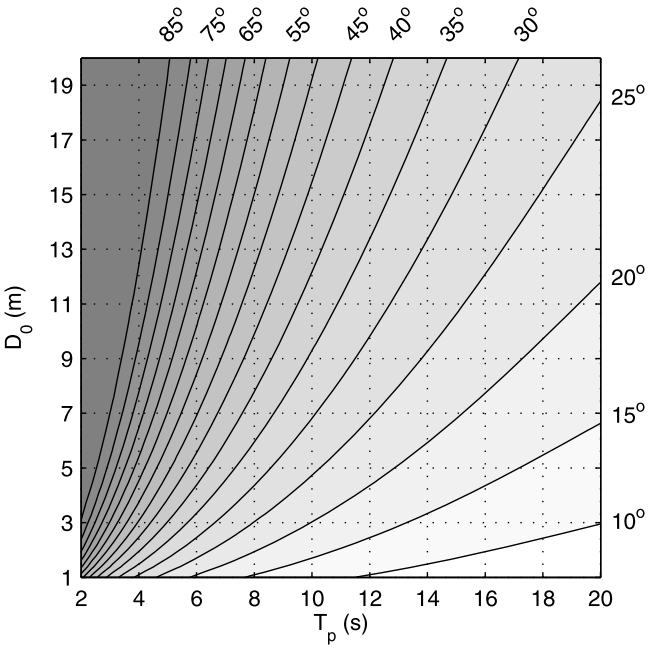

Figure 1. Maximum allowed wave angle at water depth D_0 as a function of wave period, T_p. A deep water angle $\theta_\infty = 89.9°$ is assumed at a water depth $D_\infty = 250$ m.

as the total energy flux entering the surfzone divided by the cross-shore length,

$$\mathcal{D} \sim \frac{1}{8}\rho g H_b^2 \frac{c_{gb}}{X_b}, \tag{10}$$

where g is the gravity acceleration and c_{gb} is the group celerity at breaking, computed with the shallow water assumption ($c_g \simeq \sqrt{gD}$). An estimation for the morphodynamic diffusivity is therefore,

$$\gamma_x(x,y) = \epsilon_x \gamma_b^{-1/6} g^{1/2} H_b^{11/6} X_b^{-1/3} \psi(x - x_s(y)), \tag{11}$$

where ϵ_x is a non-dimensional constant and a similar expression is used for γ_y with the constant ϵ_y. The shape function,

$$\psi(x) = \frac{1 + b + \tanh\left((X_1 - x)/L_d\right)}{1 + b + \tanh\left(X_1/L_d\right)}, \tag{12}$$

has a cross-shore distribution with a maximum in the surfzone and it decays to almost zero at the depth of closure, D_c. X_1 controls the position of D_c and is defined as $X_1 = C * X_b$, where the default value of the constant C is 2 and X_b varies with the wave height. L_d controls the length scale of the decay until X_1 and offshore of this point the shape function tends to a residual value controlled by b. The choice of the default values for ϵ_x and ϵ_y is based on the characteristic diffusion time, $T_d \sim L_d^2/\gamma_x$ and L_d^2/γ_y, of a bathymetric feature with a characteristic length L_d and the dimensional values of γ_x and γ_y are in the same order of magnitude as those corresponding to the bedslope transport in surfzone morphodynamic models [*Garnier et al.*, 2008].

[15] Notice that the cross-shore equilibrium profile is assumed to be perpendicular to the initial shoreline rather than to the evolving local shoreline orientation. Consistently, the flux given by equation (7) is assumed to be in the direction of the x-axis. The inaccuracy introduced by this approximation is not significant in the present application since changes in shoreline orientation do not exceed about 13°.

2.2. Waves

[16] For the computation of the sediment transport the wave height and direction at breaking are needed. The wave module computes the wavefield in the domain using the wave height, period and angle given at the offshore boundary, the dispersion relation,

$$\omega^2 = gk \tanh(kD), \tag{13}$$

the equation for wave number irrotationality,

$$\frac{\partial(k \sin\theta)}{\partial x} = \frac{\partial(-k\cos\theta)}{\partial y}, \tag{14}$$

and the wave energy conservation,

$$\frac{\partial}{\partial x}\left(-c_g H^2 \cos\theta\right) + \frac{\partial}{\partial y}\left(c_g H^2 \sin\theta\right) = 0. \tag{15}$$

Here $\omega = 2\pi/T_p$ is the radian frequency, T_p is the peak period, $\vec{k} = \left(k_x, k_y\right) = k(-\cos\theta, \sin\theta)$ is the wave number vector, c_g is the group celerity and θ is the angle of the wave crest with respect to the y-axis. This approach takes into account refraction and shoaling, but it neglects diffraction and dissipation by bottom shear stresses. Dissipation by breaking is not included because the wavefield is only needed up to breaking. The wavefield is computed every time step $\Delta t_w = 1$ day. There is also an option to compute the wavefield with a more detailed external wave model but this increases the computational cost and studies that included more hydrodynamic processes showed that this did not change the qualitative behavior of HAWI [*Uguccioni et al.*, 2006; *List and Ashton*, 2007].

2.3. Realistic Range of Wave Angles

[17] In theory, any wave angle is possible in infinitely deep water. However, the angle between wavefronts and coastline decreases as water depth decreases because of wave refraction. This poses an upper bound on the wave angles that are realistic at the offshore boundary of the model domain. Wave refraction depends on the wave period and shorter wave periods allow for larger angles at a given water depth.

[18] For any wave period this can be determined by assuming $\theta = \theta_\infty$ at an offshore water depth, D_∞, and refracting the waves up to the water depth of the offshore boundary, $D_0 = D(L_x)$. The angle θ_0 is found by solving equations (13) and (14). The latter reduces to the Snell law, $k_o \sin\theta_0 = k_\infty \sin\theta_\infty$, by assuming rectilinear and parallel depth contours. Taking, for example, $D_\infty = 250$ m, and $\theta_\infty \to 90°$, the angle θ_0 at D_0 gives the maximum incidence angle allowed at such depth. The results for the maximum angle as a function of wave period and D_0 are shown in Figure 1. Larger water depths in deep water, D_∞, give the same results for a wave period not larger than about 20 s.

2.4. Boundary Conditions

[19] The boundary condition,

$$\vec{q} = -\gamma_s \left(\frac{\partial z_b}{\partial x} \cos \phi_s - \frac{\partial z_b}{\partial y} \sin \phi_s + \beta_s \right) (\cos \phi_s, -\sin \phi_s), \tag{16}$$

is assumed at the shoreline, where ϕ_s is the angle between the shoreline and the y-axis. This means that the swash zone slope relaxes to an equilibrium slope β_s. If the swash slope is smaller than the equilibrium slope, sediment is transported from the wet cells to the dry cells and the shoreline advances seaward. If the swash slope is steeper, the dry beach is eroded and the shoreline retreats. The coefficient γ_s is related to the relaxation time T_s by $\gamma_s \sim (\Delta x)^2/T_s$, where Δx is the grid size.

[20] At the offshore boundary, $x = L_x$, it is assumed that the bathymetry relaxes to the equilibrium bathymetry within a certain decay distance λ_x from the boundary. At the lateral boundaries ($y = 0$, L_y) the diffusive transport is assumed to be zero and the sediment flux is controlled by the wave driven alongshore transport (equation (3)). In this sense, an open boundary condition is used, so that sediment is not necessarily conserved within the domain and the bathymetry can evolve freely. The wave driven alongshore transport depends on the local values of H_b, θ_b and ϕ. The value of ϕ at the lateral boundaries is however not obvious because it is the average surfzone orientation within a rectangle and the bathymetry outside the domain is unknown. If ϕ is determined by only using interior cells a positive feedback between the surfzone orientation and gradients in Q can arise leading to a numerical instability that causes strong accretion or erosion at the boundary. Therefore, the following boundary condition is used:

$$\frac{\partial \phi}{\partial y} = \pm (\lambda_y)^{-1} \phi \qquad y = 0, L_y. \tag{17}$$

This is consistent with an exponential decay to zero of ϕ far from the domain. The e-folding length of the decay is set to $\lambda_y = 500$ m and this has proven to lead to realistic behavior at the boundaries. In order to check the sensitivity to the lateral boundary condition, we varied the alongshore length of the domain and the area where the initial random perturbations were imposed. The results were qualitatively similar and showed that the sand waves traversed the downdrift boundary freely. The present lateral boundary condition was preferred over a periodic boundary condition because the latter would lead to artificial behavior where sand waves, leaving the domain at the downdrift boundary, would enter at the updrift boundary and interact with the beginning of the sand wavefield. Even though the general properties of the sand waves would be similar, this would lead to different dynamics and the wavelength of the sand waves would not be allowed to evolve freely (only dividers of the length of the domain).

2.5. Numerical Implementation

[21] The set of equations is discretized in space by standard finite differences on a staggered grid. Equation (1) is discretized in time by a second order Adam-Bashforth explicit method. The use of an explicit method gives a Courant-Friedrichs-Lewy stability condition of the type

$$\Delta t < cH^{-3/2} \frac{(\min\{\Delta x, \Delta y\})^2}{\max\{\epsilon_x, \epsilon_y\}}, \tag{18}$$

based on the morphological diffusivity which is roughly proportional to $H^{3/2}$. Numerical experiments show that $c \sim 0.13$ m$^{-1/2}$ s.

[22] When the shoreline deviates from a line parallel to the y-axis, jumps occur in the shoreline position. If these jumps in the shoreline position become larger than two grid cells, the sediment transport at the shoreline is not correctly evaluated. This leads to an unrealistic evolution of the shoreline and therefore there is a limitation on the maximum shoreline angle ϕ_s: $|\tan \phi_s| \leq 2\Delta x/\Delta y$. On the other hand, since the wave propagation equations are hyperbolic, it is required that a wave ray entering a cell from its offshore boundary does not exit trough a lateral boundary. This results in a constraint on $\Delta x/\Delta y$ opposite to that based on the shoreline angle: $\Delta x/\Delta y < (\tan \theta)^{-1}$. It is numerically found that $\Delta x/\Delta y \leq 1$ can be used for $\theta_0 < 55°$ but for waves up to $\theta_0 \simeq 89°$, $\Delta x/\Delta y \leq 0.25$ is required.

3. Results for Constant Wave Incidence Angle

3.1. Setup of the Default Experiment

[23] For the default experiment we used a 30 km long rectilinear coastline and constant wave conditions, $H_s = 1.41$ m, $\theta_0 = 60°$ and $T_p = 6$ s, which represent mean annual conditions that favor the development of HAWI. The size of the simulation domain was $L_x = 1.2$ km by $L_y = 30$ km, including a dry beach of 400 m width. A Dean-type profile was considered as the equilibrium profile:

$$Z(x) = -A\left((x + d)^{2/3} - d^{2/3} \right), \tag{19}$$

where d introduces a small shift to avoid an infinite slope at the shoreline. The constants d and A were chosen by prescribing the swash slope ($\beta_s = 0.03$) and the water depth, $D_{ref} = 10$ m, at the offshore distance, $x_{ref} = 700$ m. The water depth at the offshore boundary was $D_0 = 10.9$ m so that, according to section 2.3, $\theta_0 = 60°$ is the maximum allowed wave angle for a wave period $T_p = 6$ s. The mean wave conditions and the cross-shore profile were loosely based on coasts where sand waves have been observed; e.g. the Dutch coast (slightly less steep profile) and the coast of Long Island, USA (slightly longer wave periods). Random perturbations with an amplitude of $|\Delta z_b| = 0.1$ m were superimposed on the equilibrium bathymetry. These initial conditions were chosen so that the system was not forced with a specific length-scale. The other parameters used for this experiment can be found in Table 1. Sensitivity tests showed that the results were almost insensitive to changes in Δt, Δt_w and Δx. In contrast, results were quite sensitive to changes in Δy. Changing from $\Delta y = 50$ m to $\Delta y = 25$ m however had an acceptable small effect and therefore $\Delta y = 50$ m was chosen as a compromise between accuracy and computational cost. Sensitivity tests were also done for the size of the box that is used for the computation of ϕ (equation (6)). This showed that a smaller box (less

Table 1. Parameter Settings for the Default Experiment

	Parameter	Values
H_s	Offshore significant wave height	1.4 m
T_p	Offshore peak wave period	6 s
θ_0	Offshore wave angle	60°
γ_b	Breaking index	0.5
ϵ_x	Cross-shore diffusivity coefficient	0.05
ϵ_y	Alongshore diffusivity coefficient	0.05
γ_s	Swash zone diffusivity	0.001 m^2s^{-1}
X_1	Decay location cross-shore transport	2 X_b
L_d	Decay distance cross-shore transport	0.5 X_1
Δx	Cross-shore grid size	6 m
Δy	Alongshore grid size	50 m
Δt	Time step	0.001 days

smoothing) led to slightly higher growth rates but it did not affect the wavelength of the sand waves. The maximum angle of the shoreline with respect to the y-axis allowed by the grid is about 13° (tan $\phi_s = 2\Delta x/\Delta y = 0.24$, i.e. $\phi_s = 13°$).

3.2. Shoreline Evolution of the Default Experiment

[24] The initial random perturbations in the bathymetry caused small fluctuations in the shoreline position at $t = 0$ with an amplitude of about 0.5 m (Figure 2a). This is the result of the linear interpolation between the last dry cell and the first wet cell, which is used to determine the shoreline position. A Fourier analysis of the shoreline, $x_s(y, t)$, provides more information on the alongshore length scales involved in the evolution of the perturbations. The initial shoreline showed a low spectral density, spread over all length scales (Figure 2b).

[25] During the first simulated days, the small scale noise in the bathymetry was smoothed and shoreline fluctuations with a small amplitude (1 m) but larger alongshore length scale (1 km) remained. As a consequence of the model approximations and the grid size, the model does not resolve any physical processes at a length scale smaller than the width of the surfzone, i.e., smaller than 10–100 m. The initial smoothing therefore does not represent a physical process but can be considered a numerical way of generating random perturbations at a larger length scale, where the model approximations are valid. After this larger length scale was reached the simulation is considered to realistically described the morphodynamics. From this moment on the undulations amplified non uniformly. When the spacing between adjacent crests or troughs was larger, the corresponding shoreline undulation developed faster. After 25 simulated days a clear spectral peak developed at $\lambda = 2$ km and after one year wavelengths between 3 and 4 km became dominant and the amplitude of the undulations increased to about 3 m (Figures 2b and 2c).

[26] During the following years these undulations developed into a regular sand wavefield (Figure 3a). In order to quantify the dimensions and evolution of the sand waves we use the definitions presented in Figure 4. The growth rate of the amplitude of the largest sand wave, σ, can be estimated by assuming an exponential growth. The slope of a linear fit of $\log(\bar{A}(t)/\bar{A}(0))$ plotted against t gives σ (yr^{-1}). Due to the many approximations in this study and the lack of calibration, the obtained amplitudes, growth and migration rates merely give an indication of the order of magnitude and the values should only be used to compare different simulations. At $t = 6$ yr, six sand waves were present within the domain with a mean amplitude, $\bar{A}$, of about 9 m. Although the small scale undulations were still present they did not grow further and a wavelength of about 3.6 km became dominant. The other shorelines in Figure 3a show the growth and migration of the sand waves until $t = 13$ yr and Figure 3b shows the corresponding Fourier analysis of the shorelines. The amplitude of the sand waves increased until 121 m at a growth rate of about 0.36 yr^{-1}. Consistently the spectral density increased and the peak moved to $\lambda = 4.6$ km. The latter illustrates the slow increase of the wavelength of the sand waves. The sand waves migrated downdrift at a rate of about 550 m/yr. Figure 5 shows the corresponding bathymetry at $t = 13$ yr. The shoreline undulations extended into the bathymetry down to a depth of about 8 m and the fully developed sand waves tend to be slightly asymmetric in shape, so that the angle between the bathymetric lines and

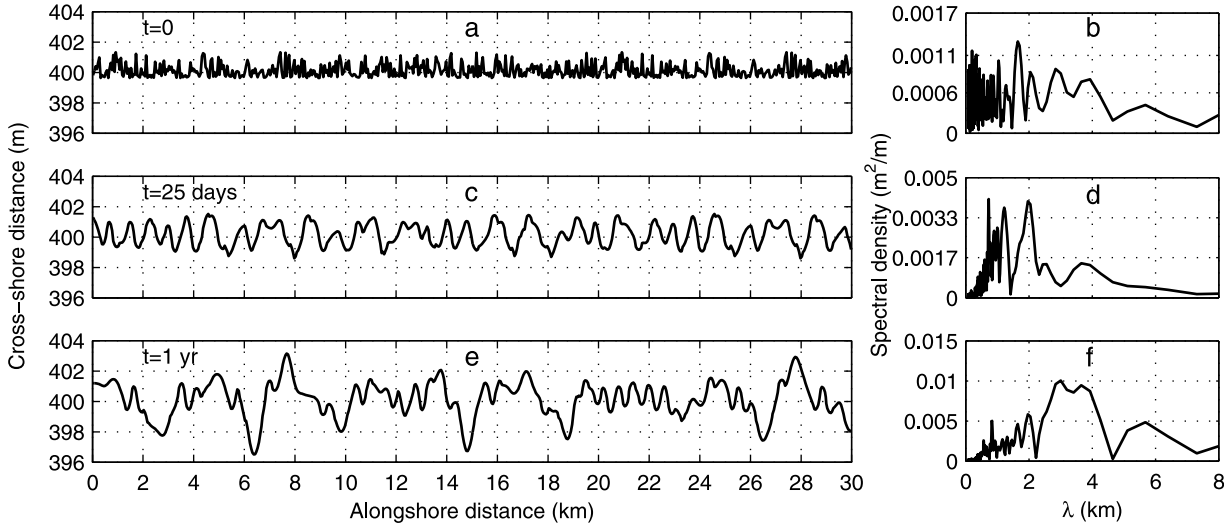

Figure 2. Shoreline evolution for the default experiment during the first year, showing (a, c, e) the initial development of shoreline instability and (b, d, f) the corresponding Fourier analysis of the shoreline. The waves come from the left in the plot and the cross-shore distance is exaggerated by a factor of 600.

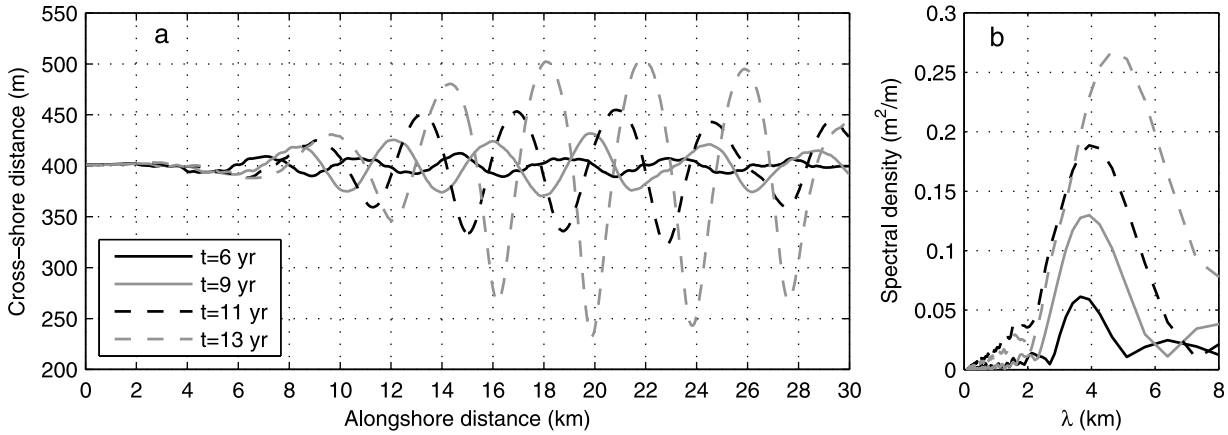

Figure 3. Shoreline evolution between 6 and 13 years, showing (a) the growth and migration of a regular sand wavefield and (b) the corresponding Fourier analysis of the shorelines. The waves come from the left and the cross-shore distance is exaggerated by a factor of 40.

the mean shoreline was larger at the downdrift slope of the crest. Interestingly the sand wave at the updrift side of the sand wavefield (located at about y = 10 km for t = 13 yr) developed much more slowly. Its amplitude merely increased from 21 m until 42 m (σ = 0.24 yr^{-1}), its wavelength was longer (5 km) and its migration celerity was lower (340 m/yr).

[27] The limitation on the shoreline angle, $|\phi_s| \leq 2\Delta x/\Delta y \sim 13°$, was exceeded after approximately 13 simulated years. After this, the predictions of the model were not reliable.

3.3. Sensitivity to Wave Incidence Angle

[28] The maximum realistic offshore wave angle of 60° was used in the default simulation. In this section we look at the sensitivity of the results to the offshore wave angle. To this end, simulations were done with θ_0 = 0°, 20°, 40°, 50° and 55°. After 13 simulated years the shoreline for θ_0 = 0 and θ_0 = 20° became straight and the bathymetric perturbations simply diffused. For θ_0 = 40° the diffusion rate was lower and a few small undulations of about 0.5 m remained from the initial noise. The behavior changed for θ_0 = 50°. The initial perturbations grew and formed small undulations of about 1.5 m amplitude with a wavelength between 3 and 4 km (Figures 6a and 6b). For θ_0 = 55° undulations developed with $\bar{A}$ = 8 m and λ = 4.5 km (Figures 6c and 6d), in contrast to the default simulation where $\bar{A}$ reached 121 m. It therefore seems that instability develops around θ_0 = 50° and that the growth rate increases rapidly with the wave angle. To confirm this we look at longer simulations with θ_0 = 50° and 55° and, after about 30 simulated years, the amplitude of the latter simulation reached about the same magnitude as in the default simulation. The growth rate was 0.17 yr^{-1} compared to 0.36 yr^{-1} for the default simulation and the migration celerity was smaller at about 365 m/yr. The simulation with θ_0 = 50° seems to really be on the limit of instability because the sand waves were consistent but hardly grew in amplitude. Even after 70 simulated years the amplitude was only about 7 m. During these years the small amplitude sand waves showed a complex behavior of migration and merging and eventually λ = 10 km became dominant.

[29] Notice that we have been looking at the wave incidence angle at the offshore boundary, where the water depth is D = 10.9 m. As will be discussed in next section, the relevant angle for HAWI is the angle at the depth of closure. According to the offshore extension of the bathymetric signal of the sand waves in the default experiment, we can assume that the depth of closure was about 8 m. For θ_0 = 50°, 55° and 60° the angle at the depth of closure was about 44°, 48° and 52°, respectively. The first value is very close to the critical angle of 42° found by *Ashton et al.* [2001] and this can explain why the instability developed around θ_0 = 50°.

3.4. Role of Cross-Shore Sediment Transport and Critical Angle for Instability

[30] In the Q2D-morfo model the cross-shore transport is represented by a diffusive transport that drives the cross-shore profile to the equilibrium profile. The cross-shore transport redistributes sediment between the dry beach, the surfzone and the shoaling zone and it is mainly governed by

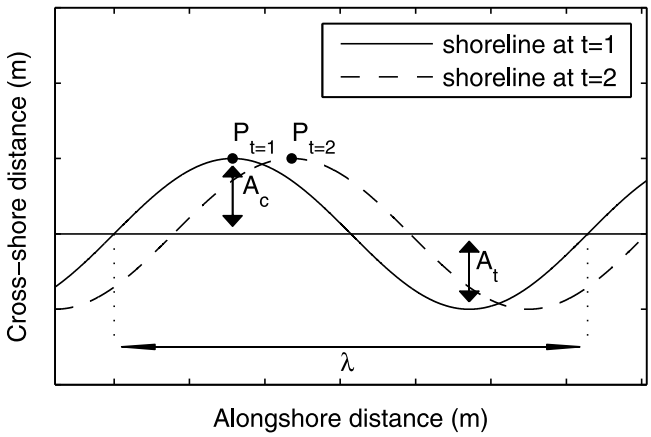

Figure 4. Definition sketch of a shoreline sand wave, where A_c is the amplitude of the crest, A_t is the amplitude of the trough, λ is the wavelength and P_t is the position of the crest. The mean amplitude is $\bar{A} = (A_c + A_t)/2$ and the migration celerity is $v = (P_{t=2} - P_{t=1})/\Delta t$.

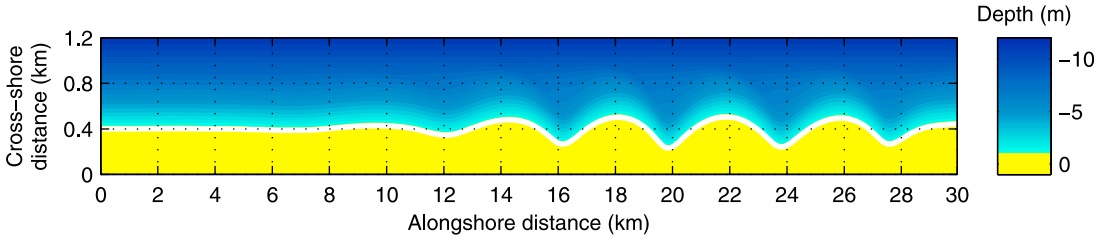

Figure 5. Contour plot for the default experiment showing the bathymetry after 13 years. The cross-shore distance is exaggerated by a factor of 4 and the waves come from the left.

the non-dimensional coefficient ϵ_x. This coefficient defines the magnitude of the diffusivity between the shoreline and the distance X_1, where the diffusivity sharply drops to a very small residual value. To investigate how cross-shore transport affects the instability, two series of experiments were done.

[31] In the first series of experiments, the effect of ϵ_x was investigated. Because the value Δt = 0.001 days of the default experiment was already close to the Courant stability condition, Δt had to be reduced for higher values of ϵ_x. The shoreline instability developed faster with increasing cross-shore diffusivity, i.e. for a faster adaptation of the cross-shore profile. The values ϵ_x = 0.01, 0.05 (default) and 0.2 resulted in growth rates of σ = 0.22, 0.36 and 0.46 yr^{-1}, respectively. Just as for the exploration of the sensitivity to the wave incidence angle the migration celerity increased with the growth rate. A very high value of ϵ_x would be equivalent to an instantaneous adaptation of the profile as used in previous studies and this would lead to an overestimation of the growth rate and the migration celerity of the shoreline sand waves.

[32] In the second series of experiments, the influence of the offshore extent of the cross-shore diffusivity profile was examined. The diffusivity profiles corresponding to different values of the ratio X_1/X_b can be seen in Figure 7a. The growth rate of the largest sand wave is also plotted as a function of X_1/X_b. For X_1/X_b = 1 only some irregular small scale undulations remained from the initial perturbations and no instability seemed to develop (after 27 simulated years). For an increasing offshore extent, instability developed and the growth rate of the sand waves increased with X_1/X_b (Figure 7c).

[33] The offshore extent of the cross-shore diffusivity profile can be related to the depth of closure, D_c, because the ratio X_1/X_b determines the depth at which the cross-shore diffusivity becomes negligible and almost no sediment transport occurs. The default experiment with X_1/X_b = 2 showed that almost no transport took place below about 8 m water depth. The diffusivity at this point was a factor 10^4 smaller than the value close to the shoreline and we use this as a criterion for D_c. With this criterion, D_c was determined for the different values of X_1/X_b and it ranged between 4.7 and 9.4 m. The wave incidence angle at these depths, θ_{Dc}, can be determined and the growth rate can be plotted as a function of θ_{Dc} (Figure 7d). It is enlightening to see that the growth rate starts to increase around 45°. It therefore seems that the critical angle required for instability should be evaluated at the depth of closure (i.e. at the most offshore extent of the bathymetric perturbation). This is in line with the exploration of the wave incidence angle in section 3.3 and with previous studies by *Falqués and Calvete* [2005], *Uguccioni et al.* [2006], and *List and Ashton* [2007], who recognized that waves must be above a critical angle at the most offshore extent of the perturbed depth contours for

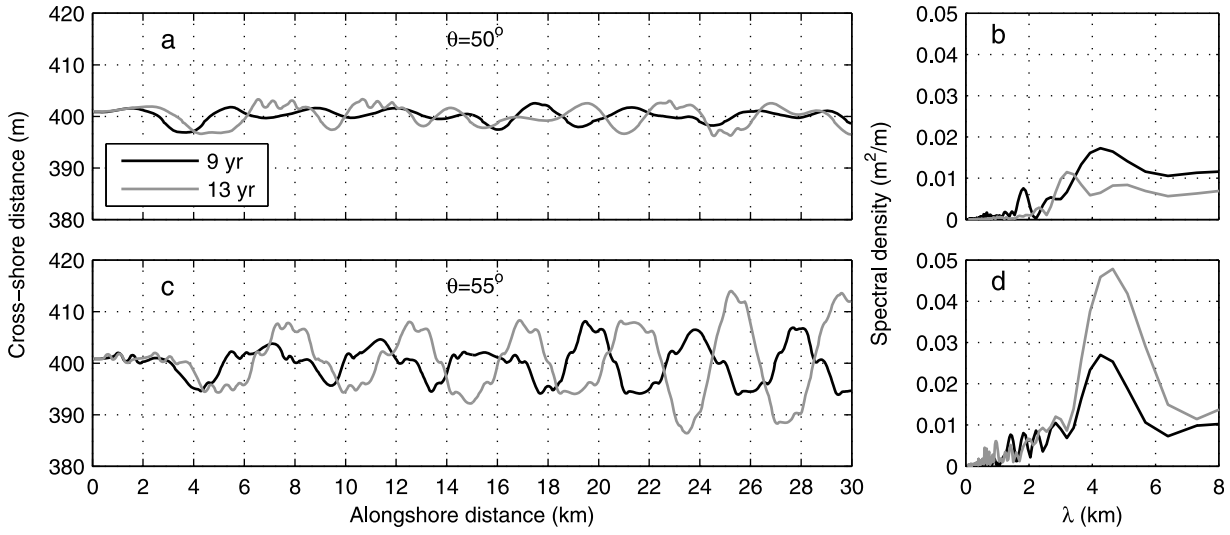

Figure 6. (a, c) The shoreline at t = 9 and 13 yr for θ_0 = 50° and 55° with (b, d) the corresponding Fourier analysis of the shorelines. The shorelines can be compared to the default experiment with θ_0 = 60° in figure 3.

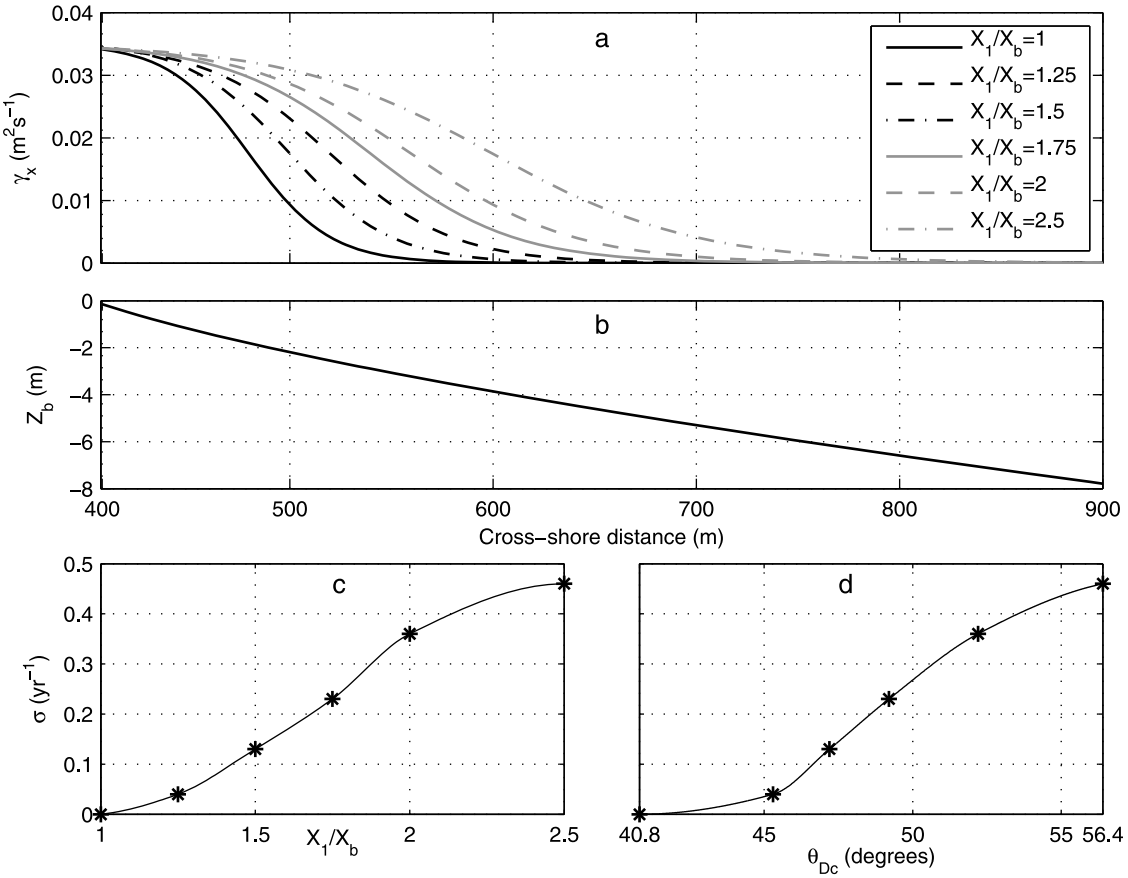

Figure 7. (a) Cross-shore diffusivity profiles as a function of X_1/X_b ratio. (b) The equilibrium beach profile. (c) Growth rate of the shoreline sand waves as a function of X_1/X_b and (d) growth rate as a function of the wave angle at the 'depth of closure' corresponding to each diffusivity profile.

HAWI to occur. Of course there is some uncertainty in this criterion because the determination of D_c is not exact. Moreover, this criterion depends on the beach conditions and the alongshore transport formula used in the model. Strictly speaking, *Ashton et al.* [2001] also evaluate the critical angle for HAWI at the most offshore extent of the shoreline perturbation but their method implicitly assumes that this extent is always until the wave base. Applying their criterion ($\theta_\infty \simeq 42^\circ$) to a real coast, where shoreline undulations, in general, extend down to a much smaller water depth, leads to an overestimation of HAWI.

3.5. Sensitivity to Wave Height and Period

[34] Results from numerical experiments with different values for H_s and T_p suggest that shoreline instability is stronger for increasing wave height and for decreasing wave period. This is the result of at least three different effects.

[35] First, instability depends on the wave angle at the depth of closure, θ_{Dc} and both an increase in wave height and a decrease in wave period lead to larger θ_{Dc}, hence to stronger instability. Wave refraction from deep water to nearshore is less intense for small wave periods so that θ_{Dc} is larger. In case of larger wave heights, D_c increases so that there is less refraction from deep water to D_c with the result that θ_{Dc} is larger. These simple physics can be used to derive a non-dimensional parameter that approximately governs the dependence of HAWI on H_s and T_p. This parameter should express the ratio between H_s and T_p that is required to keep θ_{Dc} constant for a given θ_∞. Applying the Snell Law between deep water and D_c shows that a fixed ratio between θ_∞ and θ_{Dc}, requires a constant ratio k_{Dc}/k_∞. From the dispersion relation we have,

$$\frac{4\pi^2}{T_p^2} = gk_{Dc}\tanh\left(k_{Dc}D_c\right) = gk_\infty\tanh\left(k_\infty D_\infty\right) \simeq gk_\infty. \qquad (20)$$

This means that a fixed ratio k_{Dc}/k_∞ implies that $k_{Dc}D_c$ is constant. After multiplying the left equality in equation (20) by D_c it follows that D_c/T_p^2 must be constant. By assuming that D_c is roughly proportional to H_s and after dividing by g to make it non-dimensional, we conclude that θ_{Dc} is approximately constant if H_s and T_p vary while H_s/gT_p^2 is constant. This parameter should govern the strength of HAWI, with larger values leading to a stronger instability. Notice that this parameter is similar to $s = k_\infty H_\infty$, which was used in *Falqués and Calvete* [2005]. In order to validate the relation between this parameter and HAWI, the growth rate of the sand waves was plotted as a function of H_s/gT_p^2 and it resulted into a reasonable correlation (R^2 = 0.84, not shown). Because of the large amount of simulations the growth rate was computed here by using the root mean

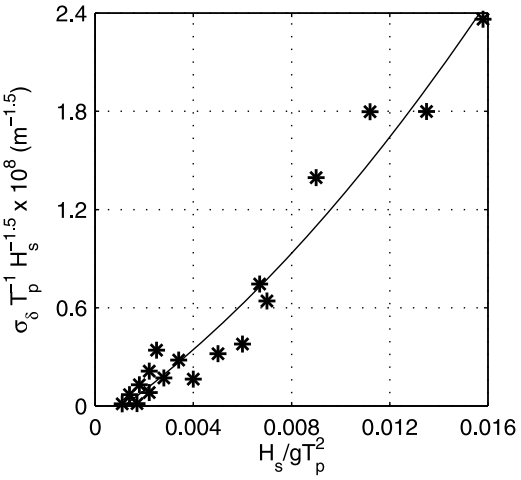

Figure 8. The initial growth rate of the shoreline sand waves (σ_δ), scaled with $T_p H_s^{1.5}$, as a function of H_s/gT_p^2. The solid line is a second order polynomial fit with $R^2 = 0.96$.

square shoreline deviation instead of the amplitude of the largest sand wave (σ_δ).

[36] Second, H_s has a direct effect on the strength of the instability. For higher waves there is more energy available and a potential instability would develop faster. According to the CERC formula (3), the sediment transport rate, Q, increases with $H_b^{2.5}$ so that by applying the one-line sediment conservation equation [*Komar*, 1998],

$$\frac{\partial x_s}{\partial t} = -\frac{1}{D_c}\frac{\partial Q}{\partial y}, \tag{21}$$

the time evolution should also increase with a factor $H_b^{2.5}$. However, D_c also increases with H_s and if we roughly assume a linear relationship, the growth rate should be scaled with $H_s^{1.5}$. After this scaling, the correlation between σ_δ and H_s/gT_p^2 increased ($R^2 = 0.91$, not shown).

[37] Finally, T_p also has a direct effect on the strength of the instability. The instability is a result of alongshore gradients in wave height produced by the differences in energy spreading between the updrift and the downdrift sides of a sand wave. The dependence of wave energy spreading on shoreline orientation is more pronounced for increasing wave period [*Falqués*, 2003]. Therefore, for a given angle at the depth of closure, θ_{Dc}, i.e., for a given value of H_s/gT_p^2, large wave periods should result in a stronger instability. This effect can be taken into account by rescaling the growth rates with a power of T_p. Figure 8 shows $\sigma_\delta T_p^{-1} H_s^{-1.5}$ as a function of H_s/gT_p^2 with $R^2 = 0.96$.

[38] Summarizing, the instability depends on H_s, T_p in a complex manner through at least three processes: i) refraction up to the depth of closure, governed by H_s/gT_s^2, ii) accelerated dynamics for increasing wave energy and iii) stronger dependence of wave energy spreading on shoreline orientation in case of high wave periods. Since the polynomial fit in Figure 8 is almost linear, we simplify the dependence as $\sigma_\delta \sim H_s^{2.5}/T_p$. Notice, that this dependence has been obtained for a particular wave angle at the offshore boundary, $\theta_0 = 60°$, and a particular cross-shore profile.

3.6. Experiments With an Initially Undulating Shoreline

[39] In this section we do not look at HAWI as a potential mechanism for the spontaneous formation of shoreline sand waves but we look at the effect of HAWI on a coast where a series of sand waves is already present. For the simulations we used an initially undulating shoreline with a typical wavelength. Because this initial shoreline is periodic we expect a uniform feedback between the shoreline and the wavefield. This will give some more insight into the self-organization process. Simulations were done with wavelengths between 1 and 10 km. The undulations are sinusoidal in the alongshore direction and have a Gaussian shape in the cross-shore direction. The amplitude of the undulations is 35 m and they extend into the bathymetry until a depth of about 7 m. A domain size of 30 km was used except for the simulation with a wavelength of 6 and 10 km, where a domain size of 40 km was used. Default parameter settings and wave conditions were used.

[40] The simulation with $\lambda = 1$ km shows that this length scale is clearly not prone to HAWI as the undulations diffused rapidly within the first 3 months ($\sigma = -8.5$ yr^{-1}). During this period the sand waves migrated downdrift at a rate of about 2700 m/yr (Figure 9b). Figure 9a shows the growth or diffusion rate of the other wavelengths. The undulations with $\lambda = 2$ km still diffused and migrated, however at a much lower rate. The simulation with $\lambda = 2.5$ km resulted in a slow growth of the shoreline undulations and it seems that around this wavelength HAWI becomes relevant. This is consistent with the minimum wavelength found with the Fourier analysis for the simulation with random perturbations. Interestingly this was the only wavelength for which the growth of the undulations slowed down after about 3 years and the amplitude seemed to become stable at about 80 m. The fastest growing wavelength was between 3 and 3.5 km.

[41] Figure 10 shows how the amplitude of the undulations increased while they migrated downdrift at a constant rate, for $\lambda = 3$ km. Just as in the previous sections the most updrift sand wave had a lower growth and migration rate and its wavelength increased. This effect died out further downdrift, where the sand waves grew and migrated uniformly and their wavelength remained constant. The growth, diffusion and migration rates in the present section were determined for these uniformly evolving undulations.

[42] For even bigger wavelengths the growth and migration rate decreased slowly (Figures 9a and 9b). The growth curve is qualitatively similar to the instability curve predicted by *Falqués and Calvete* [2005] with a linear stability analysis for similar conditions (dashed line). Even though the growth rate was low for $\lambda = 10$ km, HAWI was still relevant at this length scale. Interestingly, this simulation showed smaller scale undulations that started to grow on top of the large scale undulations after about 5 years. The first smaller scale sand wave developed at the downdrift slope of the most updrift sand wave and it triggered the growth of a sand wave train. The wavelength of these smaller scale sand waves ranged between 2 and 3 km. Because the superimposed sand wave train grew faster in amplitude and

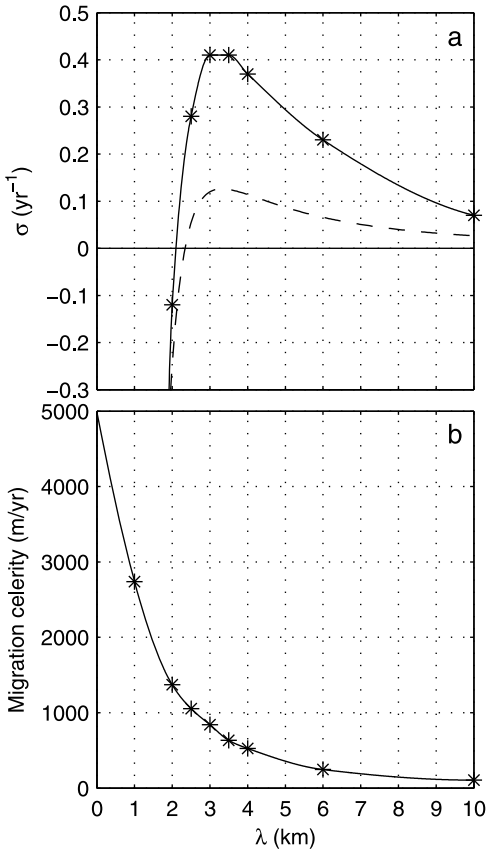

Figure 9. (a) The average growth and (b) migration rate of the sand waves of an initially undulating shoreline as a function of the wavelength of the undulations for default conditions. A negative growth rate indicates diffusion of the sand waves. The dashed line in Figure 9a is the growth curve computed with the linear stability model of *Falqués and Calvete* [2005] for similar conditions. The symbols indicate the data points associated with the simulations.

propagated faster than the large scale sand waves, it slowly consumed the larger scale sand waves.

4. Results for Variable Wave Incidence Angle

[43] In the previous sections we assumed that long term coastal evolution is driven by the mean annual wave climate, represented by one typical value for wave incidence angle, height and period. In a more realistic situation the morphological changes are the result of the net effect of varying wave conditions. In this situation high angle wave incidence alternates with low angle wave incidence, favoring coastline instability and stability, respectively. Furthermore waves can come from opposite directions and wave height and period change. It is therefore essential to look at the sensitivity of the results to more realistic wave conditions.

[44] Here we explore the effects of variable wave incidence angle by using a simplified version of the approach of *Ashton and Murray* [2006a]. We choose a representative wave incidence angle for high and low angle wave conditions ($\theta_0 = 60°$ and $\theta_0 = 30°$, respectively). The fraction of high versus low incidence angle is expressed by the variable U, where $U = 1$ ($U = 0$) means 100% high angle waves (low angle waves) and $U = 0.5$ indicates a symmetrical distribution. A second variable, A, describes the fraction of waves approaching from the left relative to mean shoreline trend versus waves approaching from the right (asymmetry), where $A = 1$ ($A = 0$) means that all waves come from the left (right). The different incidence angles that are used for a specific simulation, occur all within one simulated day. This relatively short duration is chosen to minimize chronology effects, i.e. the order in which the different wave conditions occur do not affect the shoreline evolution. We only vary the wave angle for simplicity and we use the default and constant values for H_s and T_p. Varying the wave height and period would however also affect the evolution of the shoreline because for some combinations of wave angle, height and period instability does not occur (see section 3.5).

[45] First we look at the sensitivity of the spontaneous growth of sand waves from random perturbations to different values of U (using $A = 1$). With the settings of the default simulation we find that a slight reduction of high angle waves ($U = 0.9$) strongly reduced the development of shoreline sand waves. After 20 simulated years, 4 sand waves with a wavelength of about 5 km and an amplitude of 20 m developed. This in contrast to the default simulation ($U = 1$) where sand waves with $\lambda = 4$ km and a mean amplitude up to 121 m developed within 13 years. Reducing U to 0.8 almost inhibits the development of the sand waves and merely one sand wave developed with a wavelength of 7 km and an amplitude of 5 m. For lower values of U some shoreline irregularities with an amplitude of 1 m remained from the initial small scale undulations but no sand waves developed.

[46] The present results suggest that the spontaneous formation of sand waves due to HAWI requires a wave climate with a minimum contribution of high incidence angles of about 80% and that the wavelength increases for lower fractions of high angle waves. Apparently the contribution of the diffusive effect of the low angle waves ($\theta_0 = 30°$) to the shoreline dynamics was relatively stronger than the anti-diffusive effect (growth) of the high angle waves ($\theta_0 = 60°$). This can be explained as follows. The wave angles were chosen at an equal distance from the critical incidence angle of about 45°. These are however the wave angles at the offshore boundary of the model and it is the wave angle at the depth of closure that is relevant for HAWI. The corresponding wave incidence angles at D_c were $\theta_{Dc} = 27°$ and $\theta_{Dc} = 52°$, respectively. The latter value is only just above the critical angle and the magnitude of the anti-diffusive effect was therefore small in comparison to the magnitude of the diffusive effect of the low angle waves. However, the present results might be representative for a real coast, where the range of stable wave angles is in general greater than the range of unstable wave angles (for the present study $\theta_0 \approx 0$–$50°$ and $\theta_0 \approx 50$–$60°$, respectively). This means that the net effect of the stable waves will always tend to be stronger than the net effect of unstable waves in case of $U = 0.5$ and that instability only occurs for higher values of U.

[47] The second series of simulations explores the effect of bimodal high angle waves ($U = 1$, A = variable). When a fraction of the waves came from the opposite direction ($A = 0.75$) the growth and migration rate were lower than for the default simulation ($\sigma = 0.26$ yr^{-1} and $v = 350$ m/yr) and the wavelength of the sand waves gradually increased during

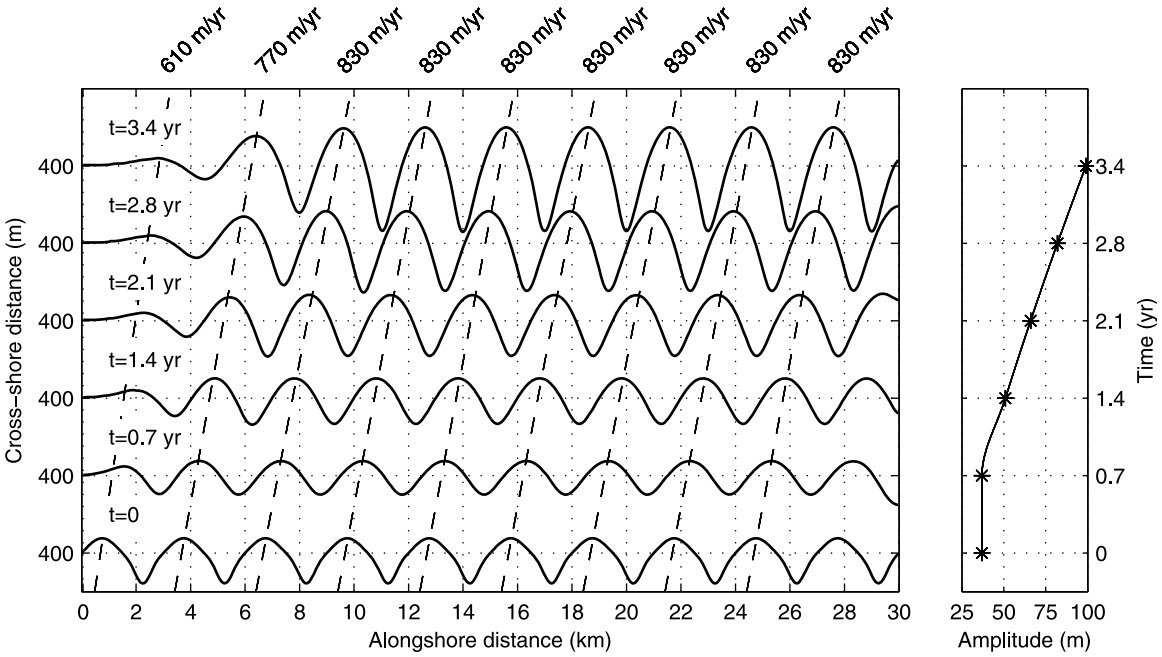

Figure 10. Uniform evolution of an undulating shoreline with an initial wavelength of 3 km for default conditions ($\theta_0 = 60°$). The migration celerity of the sand waves is indicated by the dashed lines and the growth of the mean amplitude is plotted in the right panel.

the 13 simulated years from 2 until 3 km. For $A = 0.5$ a very regular sand wavefield developed and the sand waves did not migrate. The sand waves developed initially with $\lambda =$ 2 km but after about two years the dominant wavelength started to shift to 4 km. This shift took place while the amplitudes were still small (between 1 and 4 m) and it was neither the result of a gradual stretching of the individual sand waves, nor the result of merging because both would require migration. Instead, nonlinear dynamics led to the reorganization of the sand wavefield and a subharmonic of the initial unstable undulation became dominant. In general every second crest disappeared and the initial spacing of about 2 km shifted to the more optimal spacing of about 4 km. The amplitude of these sand waves grew at a rate $\sigma = 0.26\ \mathrm{yr}^{-1}$ and their wavelength and position remained constant during the remainder of the simulation. The growth of these stationary and symmetrical sand waves is very similar to the formation of the so-called 'cuspate bumps', described by *Ashton and Murray* [2006b]. The erosion at the updrift flank and deposition at the downdrift flank was canceled out when the waves came from the opposite direction and the net change at the flanks was therefore minimal. At the crest and the trough there was a zone with accretion and erosion respectively during both conditions, which led to the growth of the crest and trough.

5. Discussion

5.1. Variable Wave Incidence Angle and Shoreline Diffusivity

[48] The results of the simulations with variable wave angles suggested that the spontaneous formation of sand waves due to HAWI requires a wave climate with a high fraction of high angle waves ($U > 0.8$). This contradicts the results of *Ashton and Murray* [2006a] who found that undulations arose from small perturbations on an initially straight coastline for $U > 0.5$. In order to understand this discrepancy we briefly discuss the approach of *Ashton and Murray* [2006a] and compare it with the present approach. *Ashton et al.* [2001] transformed equation (3) (without the second term) to a 'deep water' version, describing Q as a function of the wave height and angle at the wave base (H_∞ and θ_∞). This equation can be combined with the shoreline diffusion equation [*Pelnard-Considère*, 1956] and the diffusivity coefficient (ϵ), which indicates the magnitude of the diffusion, mainly depends on θ_∞ [*Ashton and Murray*, 2006a]. This dependance is plotted in Figure 11 (solid line). In the approach of *Ashton and Murray* [2006a], every wave angle is possible because the input waves are defined before nearshore wave transformation (at D_∞) and therefore they distributed the fraction of stable and unstable waves with a probability function over the wave angle bins, $\theta_\infty =$ 0°–45° and $\theta_\infty = 45°$–90°, respectively. The net effect for a symmetrical distribution ($U = 0.5$) can be determined by simply computing the integral of the solid line in Figure 11 and this shows that the magnitude of the positive diffusivity (low angle bin) is comparable to the magnitude of the negative diffusivity (high angle bin). This is the reason why *Ashton and Murray* [2006a] found that the shoreline was unstable for $U > 0.5$.

[49] The essential difference between the approach of the present study and that of *Ashton and Murray* [2006a] lies in the fact that in the Q2D-morfo model the perturbations extend down to D_c while in *Ashton and Murray* [2006a] down to D_∞ and, in general, $D_\infty > D_c$. For example, in our computations with $T = 6$ s, $D_c \simeq 8$ m whereas $D_\infty \simeq 30$ m. In order to illustrate the consequence of this essential difference for shoreline diffusivity, we can find the dependence of the

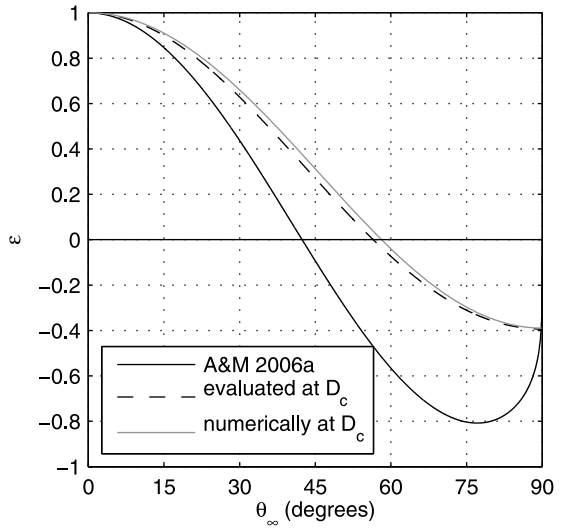

Figure 11. The shoreline diffusivity, ϵ, as a function of the deep water wave angle after *Ashton and Murray* [2006a] (solid line). The deep water angle dependance of ϵ evaluated at D_c, refracted back to deep water quantities (dashed line). The angle dependance of ϵ computed numerically at D_c, refracted back to deep water quantities (gray line).

shoreline diffusivity on θ_{Dc}. One option is to assume that the deep water equation for Q is valid at intermediate water depth (D_c) and in order to plot the dependence of ϵ on θ_{Dc} against the corresponding deep water wave angle, the waves are refracted from D_c back to deep water over a rectilinear bathymetry (Figure 11, dashed line). In this situation, the high angle wave bin is clearly smaller than the low angle bin and the magnitude of the negative diffusion is smaller. For a symmetrical distribution ($U = 0.5$), the net negative diffusion is a factor 4 smaller than the net positive diffusion. This suggests that a value of $U > 0.8$ is required for shoreline instability and the spontaneous formation of shoreline sand waves, which is consistent with the results obtained with Q2D-morfo model. A second, and more accurate method would be to express Q directly as a function of H_{Dc} and θ_{Dc}. This can not be done analytically and has therefore been done numerically [see *Falqués*, 2003] and the resulting curve (gray line) is similar to the one obtained with the first method, which demonstrates that the deep water equation for Q can indeed be applied at intermediate water depths (previously suggested by *Ashton and Murray* [2006b]).

[50] In the present study we used a mean annual value for H_0 and T_p, and D_c was therefore constant. However, in reality wave conditions vary and the instantaneous D_c will be smaller during calm conditions and bigger during storm conditions. Even though storms occur during short periods of time, they can induce strong sediment transport and the effective D_c will therefore increase with the timescale. An increase of the effective D_c would have as a consequence that the minimum value of U required for HAWI would be lower than the value of 0.8 obtained above. For very large scale shoreline features like the cuspate features and spits described by *Ashton et al.* [2001], it seems reasonable to use a large D_c (maybe even down to D_∞) because their dynamics take place on a very long timescale. However, in their simulations these large scale features developed from initially relatively small features, similar to the sand waves in the present study. The dynamics of the sand waves are relatively fast and in this case it seems more realistic to apply an effective D_c within the range used in the present study. However, the present study could be improved by basing the depth where the cross-shore sediment transport becomes negligible (see equation (14)) on a time-dependent version of the formulation of *Hallermeier* [1978], which would describe the increase of D_c with the timescale. Finally, the effect of a variable H_0 and T_p on shoreline sand wave-formation should also be addressed in future work. It is possible that a climate with alternating storm and calm conditions leads to stronger instability than a climate represented by constant averaged value.

5.2. Instability Mechanism

[51] In the context of one-line shoreline modeling, *Ashton et al.* [2001] showed that the existence of a maximum in the alongshore transport rate curve $Q(\theta_\infty - \phi)$, could lead to shoreline instability and the growth of shoreline perturbations. The actual growth of a shoreline undulation however depends on the particular transport gradients along the undulation, which are driven by the gradients in the wave height and the relative wave angle at breaking [*Ashton and Murray*, 2006a; *Falqués and Calvete*, 2005; *Falqués et al.*, 2011a]. The Q2D-morfo model can provide further insight into the physical mechanism behind HAWI and the formation of shoreline sand waves by directly looking at the 2D picture and the causes for the alongshore gradients in Q, in line with the preliminary study of *List and Ashton* [2007].

[52] Figures 12b and 12f show the alongshore distribution of Q in case of an undulating shoreline with $\lambda = 3$ km for both $\theta_0 = 60°$ and $\theta_0 = 30°$, that is, unstable and stable conditions, respectively. According to the one-line sediment conservation equation (21), $\partial Q/\partial y > 0$ ($\partial Q/\partial y < 0$) means divergence (convergence) of sediment flux, i.e., shoreline erosion (accretion). It can be seen that in case $\theta_0 = 60°$, the maximum in Q for Q2D-morfo is located slightly updrift of the crest, causing accretion at the crest and at the lee of the sand wave (solid line). This leads to growth and downdrift migration of the sand wave. In contrast, for $\theta_0 = 30°$ there is erosion at the crest and accretion at the bay, leading to diffusion of the sand wave along with a slight downdrift translation.

[53] Figures 12b and 12f also show Q for the traditional one-line approach (dashed lines). In this approach, the feedback of the morphology into the wavefield is disregarded [*Larson and Kraus*, 1991; *Komar*, 1998]. The wave height and angle at breaking are computed by wave transformation over a rectilinear bathymetry and they are therefore constant in the alongshore direction. In case $\theta_0 = 30°$, the pattern of Q is qualitatively the same for both the traditional and the Q2D-morfo approach, except for a slight lag for Q2D-morfo, that is responsible for the migration. The gradients in Q are milder for Q2D-morfo, implying a smaller diffusivity than that predicted by the traditional approach [*Ashton and Murray*, 2006a; *Falqués*, 2003; *Falqués and Calvete*, 2005]. In contrast, for $\theta_0 = 60°$, the alongshore distributions of Q for the traditional one-line approach and for Q2D-morfo are very different. The position of Q_{max} did not change for the one-line approach and the

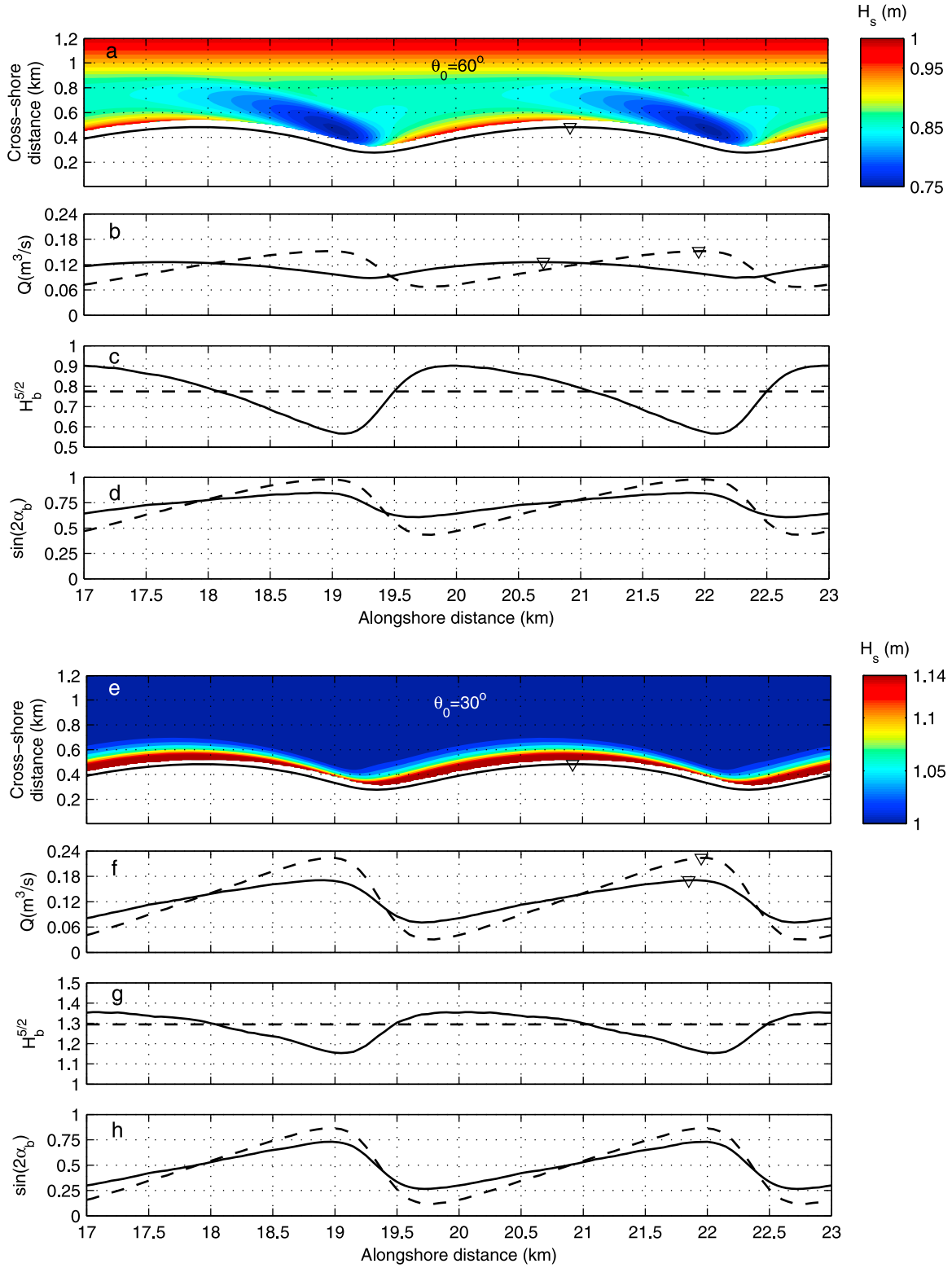

Figure 12. Contour plot of the wave height up to breaking for an undulating coastline with (a) λ = 3 km, $\theta_0 = 60°$ and (e) $\theta_0 = 30°$. The shoreline is indicated by the black line and the waves come from the left. (b and f) Alongshore distribution of the sediment transport rate Q, (c and g) $H_b^{5/2}$ and (d and h) $\sin(2\alpha_b)$. The solid lines represent the results of Q2D-morfo and the dashed lines correspond to the traditional one-line approach. The symbol ∇ indicates the maxima of the shoreline position and of Q.

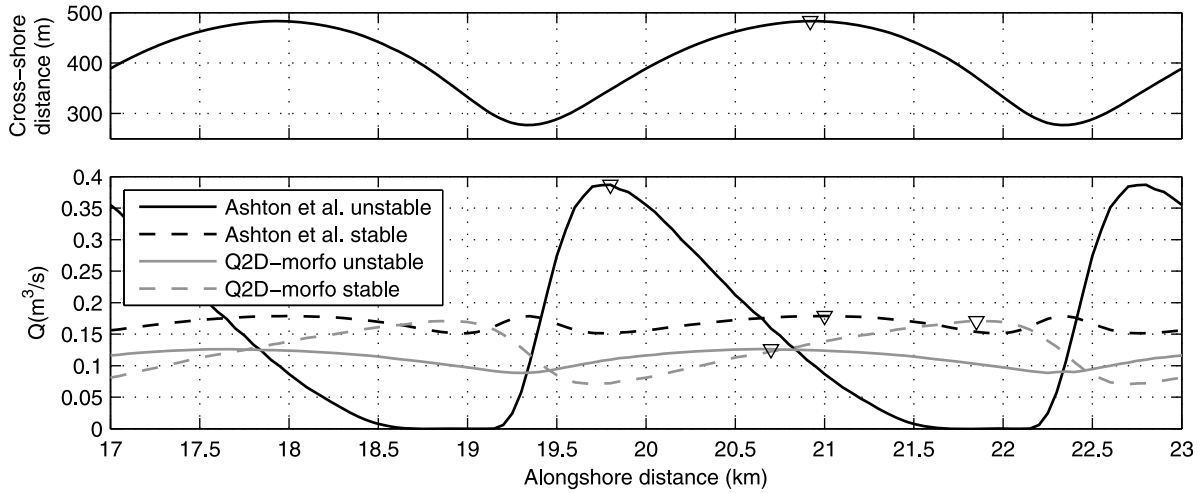

Figure 13. (top) The shoreline position of an undulating coast with $\lambda = 3$ km. (bottom) The alongshore distribution of the sediment transport rate computed with the equation of *Ashton et al.* [2001] (Q_∞) and computed with Q2D-morfo (similar to Figure 12) for stable and unstable conditions. The symbol ∇ indicates the maxima of the shoreline position and the alongshore transport.

shoreline remained stable. For the Q2D-morfo the pattern of Q changed, leading to instability.

[54] The physical cause for instability can be understood by recalling that, according to the CERC formula, Q is proportional to the product of $H_b^{5/2}$ and $\sin(2\alpha_b)$. In this section we disregard the second term in equation (3) because simulations with the parameter $r = 0$ showed that this term had little effect on the shoreline evolution. Without further investigation on the role of this term and calibration with field data it is recommended to simply not include this term in future applications of the model [see also *List et al.*, 2008]. Neglecting this term, the gradients in Q only depend on the gradients in $H_b^{5/2}$ and the gradients in $\sin(2\alpha_b)$. Figures 12c and 12g show that in both cases (unstable and stable), the H_b term has its maximum at the updrift flank of the sand wave, favoring instability. On the contrary, the α_b term has its maximum at the lee for both cases, contributing to stability. Therefore, there is in both cases a competition between the wave angle effect (stabilizing) and the wave height effect (destabilizing). For $\theta_0 = 30°$, the alongshore variations in $H_b^{5/2}$ are very mild (17% of the minimum) while the alongshore variations in $\sin(2\alpha_b)$ are very strong (114% of the minimum) with the result that the stabilizing term fully dominates the alongshore distribution of $\partial Q/\partial y$. The contrary occurs for $\theta_0 = 60°$. Now the relative variations in $H_b^{5/2}$ are bigger (57%) while the relative variations in $\sin(2\alpha_b)$ are smaller (31%). As a result, the maximum in H_b causes a shift of $Q_{\max}$ in the updrift direction so that the shoreline becomes unstable. Thus, consistently with previous studies [*Ashton and Murray*, 2006a, 2006b; *Falqués and Calvete*, 2005; *Falqués et al.*, 2011a]), our analysis shows that the essential hydrodynamic process triggering the positive feedback that causes instability is the difference in refractive energy spreading between the updrift and the downdrift flanks of the sand waves.

[55] In order to compare the present approach with that of *Ashton et al.* [2001], we compute the alongshore transport with their deep water formula (Q_∞), which is a function of H_∞ and $(\theta_\infty - \phi)$. This is similar to the 'CERC-recast' in *List and Ashton* [2007] and to obtain the wave height and angle at deep water, the waves at the offshore boundary (10.9 m depth) are transformed to deep water waves (50 m depth) by using linear wave theory and assuming a rectilinear bathymetry. The wave height and angle at deep water for unstable and stable conditions were $H_\infty = 1.73$ m, $\theta_\infty = 78.5°$ and $H_\infty = 1.12$ m, $\theta_\infty = 34.5°$, respectively. Figure 13 shows that for unstable conditions, the gradients of Q_∞ are a factor 3 bigger than those of the Q2D-morfo model, which will lead to higher growth rates. The maximum of Q_∞ is located further updrift than for Q2D-morfo and this favors growth over migration. The latter can be explained by the fact that the approach of *Ashton et al.* [2001] does not take into account the curvature of the bathymetric lines and therefore does not include the effect of wave convergence at the crest (wave focusing). This effect is described by Q2D-morfo and shifts $Q_{\max}$ closer to the crest, predicting a less unstable transport pattern. Finally, Q_∞ becomes zero at the bottom of the downdrift flank because here the relative wave angle becomes bigger than 90°, similar to the wave shadow in *Ashton and Murray* [2006a]. The simulations with Q2D-morfo show that for these relative smooth undulations with a finite cross-shore extent, a zone with zero transport is not realistic. For stable conditions (Figure 13), the gradients in Q_∞ are smaller than for the Q2D-morfo model but this seems to be the result of a secondary minimum, where the Q2D-morfo model predicts $Q_{\max}$ (at about 22 km). As a consequence, the maximum of Q_∞ is also located further updrift, only just downdrift of the crest and, this favors migration over diffusion. This secondary minimum develops because the relative wave angle at the downdrift slope becomes bigger than 42°.

[56] Even though more insight into the physical mechanism behind shoreline instability has been provided in the previous paragraph, neither the existence of a minimum length scale for the development of shoreline sand waves nor the shape of the growth curve, presented in Figure 9a, have been explained. *Falqués and Calvete* [2005] discussed the existence of a preferred wavelength for instability in the

linear regime but only provided an explanation for the minimum wavelength. Their analysis showed that for very small length scales the maximum of H_b was located downdrift of the crest and therefore the position Q_{max} was also located downdrift of the crest, which leads to diffusion. An analysis of the gradients of Q for the simulations with initially undulating shorelines with various wavelengths of section 3.6, showed that for $\lambda < 2.5$ km the position of Q_{max} was located downdrift of the crest and that for increasing wavelength the position moved updrift of the crest, leading to a shift from diffusion and migration to growth and migration. This shift was indeed caused by the shift of the position of the maximum of H_b from downdrift of the crest for wavelengths below the minimum value, to updrift of the crest for wavelengths larger than the minimum value. In addition the alongshore gradients in $H_b^{5/2}$ became relatively more important around this length scale, which contributed to the updrift shift of Q_{max}. The updrift displacement of the maximum of H_b is the result of a shift from the dominance of wave energy focusing at the crest for small wavelengths (maximum of H_b close to the crest) to the dominance of wave energy spreading for large wavelengths (maximum of H_b on the updrift slope). The reason why the approach of *Ashton et al.* [2001] does not predict a minimum wavelength, is that it does not include the effect of wave focusing.

[57] The updrift displacement of Q_{max} for increasing wavelength explains the existence of a minimum length scale for instability, but it contradicts the decreasing growth rate for larger wavelengths. The growth or diffusion rate of the undulations however does not only depend on the pattern of the alongshore transport but also on the magnitude of the alongshore gradients. Large transport gradients lead to a higher rate of growth or diffusion. The relative variations of Q decreased for increasing wavelengths and, most importantly, the absolute alongshore gradients in Q decreased due to the increase of the length scale. This can explain the decrease in growth rate for increasing wavelength and thereby the existence of an optimal wavelength for instability.

[58] Migration took place for all wavelengths (see Figure 9b) and the decrease of the migration rate with increasing wavelength can also be explained by the decreasing alongshore gradients in Q. This is in line with the general assumption that the dynamics of relatively large sandy features are slower [*Sonu*, 1968].

5.3. Qualitative Comparison With Existing Observations

[59] The role of high angle waves in the formation and dynamics of sand waves along natural coastlines is difficult to ascertain due to: i) the large length and time scales involved, ii) the scarcity of systematic measurements at these scales and iii) the confluence of other processes that may also be important (e.g., surfzone dynamics or forcing by the offshore bathymetry). Here we compare our model results with existing observations. The most relevant conclusions from our modeling study are the following. First, high angle waves cause a decrease of shoreline diffusivity that can become negative, leading to spontaneous sand wave formation due to shoreline instability. Second, sand waves develop with a wavelength in the range of 2–5 km. Third, sand waves migrate in the direction of the littoral drift with a celerity in the order of $V \sim 0.5$ km/yr and the celerity decreases with increasing wavelength. Finally, the characteristic time of the sand wave dynamics is in the order of several years.

[60] The most convincing connection between shoreline instability and high angle waves comes from elongated water bodies like lagoons or lakes [*Zenkovitch*, 1959; *Davidson-Arnott and van Heyningen*, 2003; *Ashton and Murray*, 2006b; *Ashton et al.*, 2009]. But the existence of shoreline sand waves (or erosion/accretion waves) has also been documented on several open and semi-enclosed coasts. Examples are the west coast of Denmark [*Bruun*, 1954; *Kaergaard et al.*, 2012], parts of the Dutch coast [*Verhagen*, 1989; *Ruessink and Jeuken*, 2002; *Falqués*, 2006], the barrier coast of Long Island, USA [*Thevenot and Kraus*, 1995; *Gravens*, 1999], the southern Brazilian coast [*Alves*, 2009], the northern Spanish coast [*Medellín et al.*, 2008, 2009] and the eastern Gulf of Finland [*Ryabchuk et al.*, 2011]. However, on some of the previously mentioned coasts it is unclear whether the fraction of high angle waves is big enough to cause spontaneous sand wave growth.

[61] Various studies suggest that a large and periodic input of sediment could also play a role in the formation of sand waves, e.g., discharge of river sediments [*Inman*, 1987], sediment discharged from inlets [*Thevenot and Kraus*, 1995] and the welding of shoals or oblique bars on to the shore [*Davidson-Arnott and van Heyningen*, 2003]. Where the traditional one-line modeling approach would simply predict diffusion of these large scale perturbations, the present modeling approach can explain the persistence and migration of these perturbations over a long time. This can be caused by a slight shoreline instability (e.g., only a moderate fraction of high angle waves) or merely the reduction in shoreline diffusivity compared to the traditional one-line approach. The periodicity of the perturbations and the downdrift migration could explain the formation of a sand wavefield.

[62] In addition, *van den Berg et al.* [2011] showed with the Q2D-morfo model that a single large scale perturbation (i.e., without being periodic) could lead to the formation of a sand wavefield under high angle wave conditions. Due to a chain reaction in the alongshore sediment transport gradients, a spatial instability developed, where new sand waves were formed downdrift of the initial perturbation.

[63] Care must be taken with the interpretation of the wavelengths observed in the various studies because it is not always clear how this length was defined. Some studies only report the width of the crest of a shoreline undulation [*Davidson-Arnott and van Heyningen*, 2003; *Thevenot and Kraus*, 1995]. Taking this into account the observed wavelengths (defined as in Figure 4) are in the range 1–5 km. An intriguing exception are the small sand waves along El Puntal spit, in Santander, Spain ($\lambda \sim 0.1$–0.2 km) [*Medellín et al.*, 2008]. However, *Medellín et al.* [2009] showed that HAWI may develop at such short wavelengths because of the very steep cross-shore profile and very low wave energy due to the wave sheltering. The observed migration celerity of sand waves is quite variable but it is in the same order as that predicted by the simulations at several hundreds of meters per year.

[64] Finally, we want to draw the attention to the coast of Angola and Namibia in southwest Africa. This coast features some very long uninterrupted sandy stretches associated to

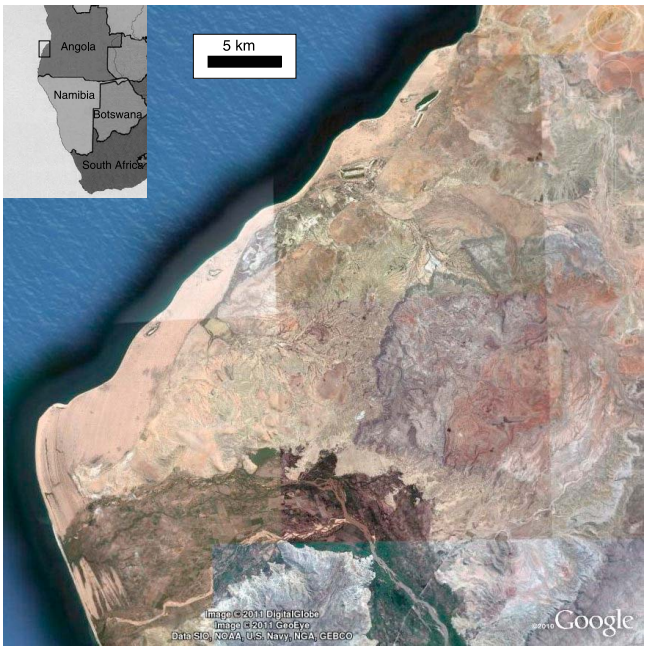

Figure 14. Shoreline sand waves with a wavelength of about 3 km along the coast of Angola, south of Baia Farta, at about 12°45′S, 13°E (Google Earth imagery © Google Inc., DigitalGlobe, and GeoEye). Used with permission.

the vast inland deserts or river deltas. The wave climate is dominated by a energetic swell from S to SW (annual mean $H_s \simeq 2$ m, with typical period T_p = 6–8 s [*Elfrink et al.*, 2003]), which is very oblique to the coast with a trend of roughly S-N. According to the HAWI theory, this coast should be very unstable and prone to generation of sand waves. *Elfrink et al.* [2003] concluded from an analysis of historical shoreline changes that HAWI plays an important role in the evolution of the Walvis Bay spit in Namibia. An exploration of satellite images reveals that shoreline sand waves are indeed very common along this coast. Figure 14 is just an example, showing a sand wavefield with six sand waves along the coast of Angola. The Coporolo delta, located in the south of the image, provides a source of sand and the sand waves are located on a stretch of coast of 20 km that is orientated NE, which results in a very large angle with respect to the average offshore wave incidence angle. The sand waves have an amplitude of about 200 m and a wavelength of about 3 km. More details and an analysis of four other sand wavefields on this coast can be found in *Falqués et al.* [2011b]. That study showed with a Fourier analysis of the shoreline position that several length scales within the range 1.5–7.5 km coexist on this coast. Even though the time evolution of the sand wavefields could not be observed, the satellite images suggest that the undulations are dynamic, showing erosion at the bays, deposition at the crest and a tendency to growth in downdrift direction. The combination of these morphological observations and the wave climate suggest that HAWI occurs on the coast of southwest Africa and that it is responsible for the generation of shoreline sand waves with wavelengths and amplitudes similar to those obtained with the model. The large scale spits that can also be found on this coast, might have formed over a very long period from the smaller scale sand waves, a process that was described by *Ashton et al.* [2001]. This process can not be reproduced by the present model due to its limitation on the angle between the shoreline and the mean coastline orientation. A different method for the updating of the shoreline should be implemented to overcome this limitation. In addition the assumption that the cross-shore transport is perpendicular to the mean coastline orientation and not to the local bathymetric lines is only valid for relatively small amplitude features.

6. Conclusions

[65] A quasi 2D morphodynamic model for large scale shoreline dynamics is presented and used to study shoreline instability and the dynamics of shoreline sand waves. Simulations with constant high angle wave incidence show that shoreline sand waves can develop in unison from small perturbations on a rectilinear coastline. Consistent with previous modeling studies, the minimum incidence angle that leads to high angle wave instability is about 45° but it is shown here that this angle is required at the depth of closure (i.e., the most offshore reach of shoreline perturbations) and not at deep water, which is how the study of *Ashton et al.* [2001] is commonly interpreted. The growth rate of the shoreline sand waves increases strongly with angles above the threshold value and the growth is favored by high waves and short wave periods, with the growth rate being roughly proportional to $H_s^{2.5} T_p^{-1}$.

[66] In the generic numerical experiments shoreline sand waves develop with wavelengths between 2 and 5 km. The timescale for the sand wave formation is in the order of several years. The amplitude of the sand waves increases exponentially due to the positive feedback between morphological changes and the wavefield and the sand waves migrate downdrift at a rate of about 0.5 km/yr.

[67] Cross-shore dynamics plays an important role in the feedback between shoreline perturbations and the wavefield because it determines if a perturbation reaches into the bathymetry down to a depth where the wave angle is greater than the threshold value. Faster cross-shore dynamics leads to higher growth rates.

[68] Simulations with wave incidence angle alternating between low and high angles (30° and 60°, respectively) show that even a small proportion of low wave angles strongly reduces shoreline instability. Contrary to previous studies we find that instability requires a wave climate with a minimal proportion of high angle wave incidence of at least 80%. The latter is essentially the consequence of a more restricted offshore extent of the bathymetric signal of the shoreline sand waves in present study. A wave climate with high wave angles alternating between opposite directions reduces shoreline instability and, in case the wave climate is completely symmetrical, the sand waves do not migrate and organize themselves with a constant wavelength.

[69] An analysis of the pattern of alongshore transport, wave height and relative wave angle along an undulating coastline gives more insight into the instability mechanism and wavelength selection. It confirms that wave energy spreading due to refraction is essential for high angle wave instability. Moreover, it was found that the alongshore transport pattern shifts from diffusion and migration to growth and migration for a minimum wavelength of the

undulations. Therefore undulations with small length scales diffuse even under high angle wave conditions. At the same time the gradients in alongshore transport decrease for increasing wavelength, leading to decreasing growth rates. This explains the existence of a optimal length scale for sand wave growth of several kilometers.

[70] This study does not intend to model observed sand waves along any particular coast but we investigate the basic physics and general characteristics of sand waves emerging from HAWI. Nevertheless, the morphological and hydrodynamic conditions used for the numerical experiments may be representative for many coasts where high angle waves are dominant. Existing observations of sand waves and the exploration of satellite images from the southwest coast of Africa show that sand waves are frequently present where wave incidence is very oblique. The length scale, growth time and migration celerity of the modeled sand waves are consistent with these observations.

[71] **Acknowledgments.** This research has been funded by the Spanish Ministerio de Ciencia e Innovación, through the research project 'Modelización y monitorización integradas en morfodinámica de playas naturales y regeneradas' (CTM2009-11892/IMNOBE). The first author is supported by a FPI scholarship of the Spanish government within the research project CTM2006-08875/MAR. The authors would like to thank the three reviewers and the editors for their constructive comments, which helped to improve this paper.

References

Alves, A. R. (2009), Long term erosional hot spots in the southern Brazilian coast, *J. Geophys. Res.*, *114*, C02020, doi:10.1029/2008JC004933.

Ashton, A., and A. B. Murray (2006a), High-angle wave instability and emergent shoreline shapes: 1. Modeling of sand waves, flying spits, and capes, *J. Geophys. Res.*, *111*, F04011, doi:10.1029/2005JF000422.

Ashton, A., and A. B. Murray (2006b), High-angle wave instability and emergent shoreline shapes: 2. Wave climate analysis and comparisons to nature, *J. Geophys. Res.*, *111*, F04012, doi:10.1029/2005JF000423.

Ashton, A., A. B. Murray, and O. Arnault (2001), Formation of coastline features by large-scale instabilities induced by high-angle waves, *Nature*, *414*, 296–300.

Ashton, A. D., A. B. Murray, R. Littlewood, D. A. Lewis, and P. Hong (2009), Fetch-limited self-organization of elongate water bodies, *Geology*, *37*, 187–190.

Battjes, J. A. (1975), Modeling of turbulence in the surfzone, in *Proceedings of the Symposium on Modelling Techniques*, pp. 1050–1061, Am. Soc. of Civ. Eng., New York.

Bruun, P. (1954), Migrating sand waves or sand humps, with special reference to investigations carried out on the Danish North Sea Coast, in *Proceedings of the International Conference on Coastal Engineering*, pp. 269–295, Am. Soc. of Civ. Eng., New York.

Castelle, B., B. Ruessink, P. Bonneton, V. Marieu, N. Bruneau, and T. Price (2010), Coupling mechanisms in double sandbar systems. Part 1: Patterns and physical explanation, *Earth Surf. Processes Landforms*, *35*, 476–486, doi:10.1002/esp.1929.

Coco, G., and A. B. Murray (2007), Patterns in the sand: From forcing templates to self-organization, *Geomorphology*, *91*, 271–290.

Cooper, J., and O. Pilkey (2004), Longshore drift: Trapped in an expected universe, *J. Sediment. Res.*, *74*, 599–606.

Davidson-Arnott, R. G. D., and A. van Heyningen (2003), Migration and sedimentology of longshore sandwaves, Long Point, Lake Erie, Canada, *Sedimentology*, *50*, 1123–1137.

Elfrink, B., G. Prestedge, C. B. M. Rocha, and J. Juhl (2003), Shoreline evolution due to highly oblique incident waves at Walvis bay, Namibia, paper presented at 5th International Symposium on Coastal Engineering and Science of Coastal Sediment Processes, Coastal Sediments 03, Clearwater Beach, Florida.

Falqués, A. (2003), On the diffusivity in coastline dynamics, *Geophys. Res. Lett.*, *30*(21), 2119, doi:10.1029/2003GL017760.

Falqués, A. (2006), Wave driven alongshore sediment transport and stability of the Dutch coastline, *Coastal Eng.*, *53*, 243–254.

Falqués, A., and D. Calvete (2005), Large scale dynamics of sandy coastlines: Diffusivity and instability, *J. Geophys. Res.*, *110*, C03007, doi:10.1029/2004JC002587.

Falqués, A., D. Calvete, and F. Ribas (2011a), Shoreline instability due to very oblique wave incidence: Some remarks on the physics, *J. Coastal Res.*, *27*(2), 291–295.

Falqués, A., N. van den Berg, F. Ribas, and M. Caballeria (2011b), Modelling shoreline sand waves. application to the coast of Namibia, paper presented at 7th Symposium on River, Coastal and Estuarine Morphodynamics, Int. Assoc. for Hyrdro-Evnviron. Eng., Beijing, China.

Garnier, R., D. Calvete, A. Falqués, and N. Dodd (2008), Modelling the formation and the long-term behavior of rip channel systems from the deformation of a longshore bar, *J. Geophys. Res.*, *113*, C07053, doi:10.1029/2007JC004632.

Gravens, M. B. (1999), Periodic shoreline morphology, Fire Island, New York, in *Coastal Sediments '99*, edited by N. Kraus and W. McDougal, pp. 1613–1626, Am. Soc. Civ. Eng., Reston, Va.

Guillen, J., M. J. F. Stive, and M. Capobianco (1999), Shoreline evolution of the Holland Coast on a decadal scale, *Earth Surf. Processes Landforms*, *24*, 517–536.

Hallermeier, R. J. (1978) Uses for a calculated limit depth to beach erosion, in *Coastal Engineering 1978*, pp. 1493–1512, Am. Soc. of Civ. Eng., Reston, Va.

Inman, D. L. (1987), Accretion and erosion waves on beaches, *Shore Beach*, *55*(3/4), 61–66.

Kaergaard, K., J. Fredsoe, and S. B. Knudsen (2012), Coastline undulations on the West Coast of Denmark: Offshore extent, relation to breaker bars and transported sediment volume, *Coastal Eng.*, *60*, 109–122.

Komar, P. D. (1998), *Beach Processes and Sedimentation*, 2nd ed., Prentice Hall, Englewood Cliffs, N. J.

Larson, M., and N. C. Kraus (1991), Mathematical modeling of the fate of beach fill, *Coastal Eng.*, *16*, 83–114.

List, J. H., and A. D. Ashton (2007), A circulation modeling approach for evaluating the conditions for shoreline instabilities, in *Coastal Sediments 2007*, pp. 327–340, Am. Soc. of Civ. Eng., Reston, Va.

List, J. H., L. Benedet, D. M. Hanes, and P. Ruggiero (2008), Understanding differences between Delft3d and emperical predictions of alongshore sediment transport gradients, in *Coastal Engineering 2008*, pp. 1864–1875, World Sci., Hackensack, N. J.

Medellín, G., R. Medina, A. Falqués, and M. González (2008), Coastline sand waves on a low energy beach at 'El Puntal' spit, Spain, *Mar. Geol.*, *250*, 143–156.

Medellín, G., A. Falqués, R. Medina, and M. González (2009), Sand waves on a low-energy beach at El 'Puntal' spit, Spain: Linear stability analysis, *J. Geophys. Res.*, *114*, C03022, doi:10.1029/2007JC004426.

Ozasa, H., and A. H. Brampton (1980), Mathematical modelling of beaches backed by seawalls, *Coastal Eng.*, *4*, 47–63.

Pelnard-Considère, R. (1956), Essai de theorie de l'evolution des formes de rivage en plages de sable et de galets, in *4th Journees de l'Hydraulique, Les Energies de la Mer, Paris*, pp. 289–298, Soc. Hydrotech. de France, Paris.

Ruessink, B. G., and M. C. J. L. Jeuken (2002), Dunefoot dynamics along the dutch coast, *Earth Surf. Processes Landforms*, *27*, 1043–1056, doi:10.1002/esp.391.

Ryabchuk, D., I. Leont'yev, A. Sergeev, E. Nesterova, L. Sukhacheva, and V. Zhamoida (2011), The morphology of sand spits and the genesis of longshore sand waves on the coast of the eastern Gulf of Finland, *Baltica*, *24*(1), 13–24.

Short, A. D. (1999), *Handbook of Beach and Shoreface Morphodynamics*, Wiley, Chichester, U. K.

Sonu, C. J. (1968), Collective movement of sediment in littoral environment, in *Coastal Engineering 1968*, pp. 373–400, Am. Soc. of Civ. Eng., Reston, Va.

Stewart, C. J., and R. G. D. Davidson-Arnott (1988), Morphology, formation and migration of longshore sandwaves; Long Point, Lake Erie, Canada, *Mar. Geol.*, *81*, 63–77.

Stive, M. J. F., S. G. J. Aarninkhof, L. Hamm, H. Hanson, M. Larson, K. M. Wijnberg, R. J. Nicholls, and M. Capobianco (2002), Variability of shore and shoreline evolution, *Coastal Eng.*, *47*, 211–235.

Thevenot, M. M., and N. C. Kraus (1995), Longshore sandwaves at Southampton Beach, New York: Observations and numerical simulation of their movement, *Mar. Geol.*, *126*, 249–269.

Uguccioni, L., R. Deigaard, and J. Fredsoe (2006), Instability of a coastline with very oblique wave incidence, in *Coastal Engineering 2006*, pp. 3542–3553, World Sci., Hackensack, N. J.

van den Berg, N., A. Falqués, and F. Ribas (2011), Long-term evolution of nourished beaches under high angle wave conditions, *J. Mar. Syst.*, *88*, 102–112.

Verhagen, H. J. (1989), Sand waves along the dutch coast, *Coastal Eng.*, *13*, 129–147.

Zenkovitch, V. P. (1959), On the genesis of cuspate spits along lagoon shores, *J. Geol.*, *67*, 269–277.